# Quasielastic scattering of light exotic nuclei

O. M. Knyaz'kov
*St. Petersburg State University, St. Petersburg*

I. N. Kukhtina
*Joint Institute for Nuclear Research, Dubna*

S. A. Fayans
*Kurchatov Institute, Moscow*

Fiz. Élem. Chastits At. Yadra **28**, 1061–1114 (July–August 1997)

The recent experimental data on the quasielastic scattering of light unstable nuclei on stable target nuclei are reviewed. The microscopic approaches to the construction of the nucleon density distributions in nuclei and the projectile–target interaction potentials are described. The cross sections for quasielastic scattering are analyzed for a large group of light exotic nuclei. The problem of the existence of a neutron or proton halo in nuclei and other features of the nuclear matter distribution are discussed. Possible future experiments on quasielastic scattering and other reactions using radioactive beams are suggested. © *1997 American Institute of Physics.* [S1063-7796(97)00504-4]

## INTRODUCTION

The intensive use of radioactive beams in the last ten years has led to the discovery of a number of unusual properties of light exotic nuclei, i.e., nuclei far from the $\beta$-stability line (see, for example, the reviews of Refs. 1–4 and references therein). Analysis of the cross sections for the interaction of He, Li, and Be isotopes with large neutron excess with stable target nuclei at intermediate energies has indicated the presence of an extended neutron density-distribution tail. This effect is especially clear for $^{11}$Li, which, according to the additional information about the $^{11}\text{Li}\rightarrow{}^{9}\text{Li}+2n$ fragmentation cross sections and the $^{9}$Li momentum distribution in this reaction, shows that the $^{11}$Li nucleus possesses a neutron halo. The existence of a neutron halo has also been confirmed for $^{6}$He, $^{8}$He, and $^{11}$Be. In Ref. 5 a similar phenomenon was discovered for $^{8}$B, which has a proton excess. Further studies showed that in this case there is either a proton halo or a sizable proton skin.

The elastic scattering of light exotic nuclei at energies from 20 to 100 MeV/nucleon, on the one hand, gives information additional to that provided by experiments on fragmentation, breakup, nucleon transfer, Coulomb dissociation, etc. On the other hand, it gives specific information about the effect on the cross section of the interaction potential between an exotic projectile and the target nucleus, and in a microscopic analysis it provides information about the matter density distribution in the exotic nucleus. Therefore, there is reason to think that the elastic scattering of light exotic nuclei can serve as an indicator of the properties of the nucleon halo. The first arguments for this were presented in Ref. 6. Various methodological studies of the expected properties of the interaction potentials of light exotic nuclei and their scattering on stable target nuclei are described in Ref. 4. However, when that review[4] went to press there were no reliable experimental data on the elastic scattering of light exotic nuclei, and so actual experimental situations were not reflected there. Two reviews[7,8] have recently appeared in which the properties of the structure of light exotic nuclei are analyzed.

By now, experiments have been performed at various sites to obtain the angular distributions of the elastic scattering of $^{11}$Li on $^{28}$Si at 29 MeV/nucleon (Ref. 9), $^{11}$Li on $^{12}$C at 60 MeV/nucleon (Ref. 10), $^{12}$Be and $^{14}$Be on $^{12}$C at 56 MeV/nucleon (Ref. 11), and $^{7}$Be and $^{8}$B on $^{12}$C at 40 MeV/nucleon (Ref. 12). We note that in all these cases the experimental conditions are such that the contributions of elastic and inelastic processes to the angular distributions are not separated. Therefore, the experimentally studied processes can be referred to as quasielastic scattering. In addition to these quasielastic scattering reactions, there have also been experimental studies in the inverse kinematical regime of the elastic scattering of $^{9}$Li and $^{11}$Li nuclei with energies 60 and 62 MeV/nucleon, respectively, on protons[13] and of $^{8}$He nuclei at energy 73 MeV/nucleon on protons.[14] The angular distributions of the elastic scattering of $^{11}$Li at energy 75 MeV/nucleon and of $^{8}$He at 66 MeV/nucleon on protons have recently been measured.[15] The elastic scattering of $^{6}$He and $^{8}$He on protons at intermediate energies has been studied in Refs. 16 and 17. The angular distributions for the elastic scattering of $^{10}$Be and $^{11}$Be on protons at 59.3 and 49.3 MeV/nucleon, respectively, have been obtained in Ref. 18.

Various theoretical approaches have been applied to these reactions: the standard optical model with fitted parameters,[19] the optical model with potentials calculated microscopically (see, for example, Ref. 20), and the Glauber approximation.[21] In those cases (the folding model and the Glauber approximation) where the scattering cross sections were analyzed on the basis of information about the matter density distribution in the nucleus, they were calculated using various nuclear-structure models. Among the other approaches to solving this problem is the density-functional method,[22] in which the neutron and proton densities for both the target nucleus and the projectile are calculated on a unified basis.

Along with the angular distributions of elastically scat-

 1063-7796/97/040418-22$10.00  

tered particles, another quantity sensitive to the optical potential is the total reaction cross section $\sigma_R$. Experimental data on $\sigma_R$ at various energies are available for a number of light exotic nuclei.

The goal of the present study is to analyze the available experimental data on the elastic scattering of light exotic nuclei and the corresponding total reaction cross sections. In Sec. 1 we discuss the various theoretical approaches for describing the mechansims of elastic scattering of light exotic nuclei and the theoretical schemes for calculating the neutron and proton density distributions in these nuclei. In Sec. 2 we analyze the experimental data on the quasielastic and elastic scattering of these nuclei and present the results of calculations of the total reaction cross sections. In Sec. 3 we discuss the appearance of a soft dipole mode in connection with the phenomenon of the nucleon halo. In the Conclusion we summarize the results and discuss further possibilities for studying the properties of light exotic nuclei by means of experiments on elastic scattering and other nuclear reactions.

## 1. THEORETICAL MODELS

It is natural to analyze elastic scattering in the potential approach, using a complex optical potential. The general theory of the optical potential was developed by Feshbach.[23,24] According to it, the generalized optical potential is given by

$$V_{\text{opt}}=\langle\varphi_0|V|\varphi_0\rangle+\langle\varphi_0|V\hat{Q}(E-H_{QQ})^{-1}\hat{Q}V|\varphi_0\rangle. \quad (1)$$

Here $\varphi_0$ is the ground-state wave function of the colliding nuclei, $V$ is the interaction between the projectile and target nuclei, $\hat{Q}$ is an operator which projects the exact wave function of the entire system onto the subspace of inelastic and closed channels, $E$ is the total energy of the system of projectile plus target nucleus, and $H_{QQ}$ is the projection of the total Hamiltonian of the entire system onto the $Q$ subspace. If the interaction $V$ is written as a sum of effective nucleon–nucleon forces, the first term in (1) will be of first order in the effective forces, and the second term will contain terms of second and higher order.

In the standard macroscopic model the entire expression (1) is replaced by a complex, local, energy-independent potential with parameters determined from comparison of the theoretical and experimental angular distributions of the elastically scattered particles. In the microscopic approach the first term in (1) is calculated using information about the effective forces and the matter density distribution in the nuclei, and the second term is usually omitted. If the effective forces are real, the second term completely determines the imaginary part of the optical potential and represents an addition to the real part of the potential. This addition is referred to as the polarization potential, because it is related to excitation effects ("polarization of the core") in nuclear scattering. Its inclusion in the optical potential represents going beyond the "frozen"-nucleon approximation.

The calculation of the second term in (1) is an extremely complicated problem, and so the polarization potential is often either completely omitted, or somehow parametrized.

### 1.1. The macroscopic optical model

The standard potential of the phenomenological optical model has the form

$$U_{\text{opt}}(r)=-V_R f_R(r)-iW_v f_I(r)+4ia_I W_s(d/dr)f_I(r)+2(\hbar/m_\pi c)^2\cdot 1/r\cdot(d/dr)V_{LS}f_S(r)(\mathbf{LS})+V_{\text{coul}}(r), \quad (2)$$

$$R_i=r_i A^{1/3},\quad f_i(r)=(1+\exp((r-R_i)/a_i))^{-1},\quad i=R,I,LS. \quad (2a)$$

Here the first term is the central part of the real potential, the second and third terms are the volume and surface absorption potentials, and the next term is the spin–orbit term. The last term in (2) is usually written as the Coulomb interaction of two charged spheres. The scheme of analyzing the elastic and inelastic scattering cross sections with the potential (2) and using a fit with $\chi^2$ minimization possesses a certain simplicity. However, in the case of light exotic nuclei it rarely leads to a successful description of the experimental data. This is because in Eq. (2) the radial dependence of all the form factors is fixed and is the Woods–Saxon dependence. However, already in the case of nucleons and $\alpha$ particles it has been shown[25,26] that the potential constructed using effective forces differs from the Woods–Saxon form.

Nevertheless, analysis of the elastic scattering of light exotic nuclei using the phenomenological optical model can be meaningful, because it tells how strongly the properties of the optical potential of an exotic nucleus differ from those of the potential of an adjacent stable nucleus (for example, $^{11}$Li versus $^{11}$C or $^{6}$He versus $^{6}$Li). Some of the results of such an analysis will be presented below in Sec. 2.

### 1.2. The microscopic optical model

Let us consider the interaction of two composite particles. In first order in the effective nucleon–nucleon forces the interaction potential can be written as a sum

$$U(\mathbf{R})=U^E(\mathbf{R})+U^D(\mathbf{R}), \quad (3)$$

where $U^D(\mathbf{R})$ is the direct potential of the double-folding model:[19]

$$U^D(\mathbf{R})=\int\int\rho^{(1)}(\mathbf{r}_1)V^D(\mathbf{s})\rho^{(2)}(\mathbf{r}_2)d\mathbf{r}_1 d\mathbf{r}_2. \quad (4)$$

Here $V^D(\mathbf{s})$ is the direct component of the effective interaction, $\mathbf{s}=\mathbf{r}_2-\mathbf{r}_1+\mathbf{R}$, and $\rho^{(i)}(\mathbf{r}_i)$ are the densities of the colliding nuclei ($i=1,2$). The main contribution to the "exchange" potential $U^E(\mathbf{R})$ comes from one-nucleon exchange effects, which can be described in the density-matrix formalism:[27]

$$U^E(\mathbf{R})=\int\int\rho^{(1)}(\mathbf{r}_1,\mathbf{r}_1+\mathbf{s})V_E(\mathbf{s})\rho^{(2)}(\mathbf{r}_2,\mathbf{r}_2-\mathbf{s})\times\exp(i\mathbf{k}(\mathbf{R})\mathbf{s}/\eta)d\mathbf{r}_1 d\mathbf{r}_2. \quad (5)$$

This is the localized form of the exchange term. Here $V_E(\mathbf{s})$ is the exchange component of the effective interaction, $\rho^{(i)}\times(\mathbf{r},\mathbf{r}')$ are the density matrices of the colliding nuclei ($i=1,2$),

$$\rho^{(i)}(\mathbf{r},\mathbf{r}')=\sum_k \varphi_k(\mathbf{r})\varphi_k^*(\mathbf{r}'), \tag{6}$$

$\mathbf{k}(\mathbf{R})$ is the local momentum given by

$$k^2(\mathbf{R})=(2m\eta/\hbar^2)(E-U(\mathbf{R})-V_c(\mathbf{R})), \tag{7}$$

where

$$\eta=\frac{A_1A_2}{A_1+A_2}, \tag{7a}$$

$A_i$ ($i=1,2$) are the nuclear mass numbers, and $V_c(\mathbf{R})$ is the Coulomb potential. The calculation of the density matrix using the one-particle expression (6) is rather complicated, and so $\rho(\mathbf{r},\mathbf{r}')$ is usually calculated using the modified Slater approximation, which has been validated in the description of the interaction of nucleons, $\alpha$ particles, and heavy ions with nuclei:[28]

$$\rho(\mathbf{r},\mathbf{r}+\mathbf{s})=\rho\left(\mathbf{r}+\frac{\mathbf{s}}{2}\right)\hat{j}_1\left(k_{\text{eff}}\left(\mathbf{r}+\frac{\mathbf{s}}{2}\right)s\right). \tag{8}$$

Here $\hat{j}_1(x)$ is the exchange correlator. For $s\to 0$, i.e., in the approximation of zero interaction range, $\hat{j}_1(x)\to 1$. The effective momentum $k_{\text{eff}}$ includes boundary effects and coincides with the local Fermi momentum in infinite nuclear matter. Expressions for $\hat{j}_1(x)$ and $k_{\text{eff}}$ can be found in Ref. 28. It follows from Eq. (5) that an iteration procedure is necessary for constructing $U^E(R)$, because $U^E(R)$ also enters into the right-hand side of this expression via $k(\mathbf{R})$ [see Eqs. (7) and (3)].

Let us briefly discuss the application of the density-matrix formalism for analyzing scattering processes. This formalism was first used in Ref. 29 to describe inelastic proton scattering on deformed nuclei. An iteration-free scheme for calculating the exchange potential was developed in Ref. 30. It allowed the explicit construction of the contribution of exchange effects to the nucleon–phonon interaction[31] and the use of the density-matrix formalism for describing the inelastic scattering of nucleons and $\alpha$ particles on vibrational nuclei.[32–34] In Refs. 35 and 36 an iteration-free procedure was developed for Eq. (5) and used to analyze nuclear-rainbow effects in the elastic and inelastic scattering of $\alpha$ particles on nuclei (see also Ref. 37). However, analysis showed that in the case of heavier projectiles, small $R$, and low energies the iteration procedure is more accurate, and it was used in the subsequent applications of the density-matrix formalism for describing scattering processes.[20,38]

To isolate explicitly the isospin dependence of the potential, we introduce the isoscalar $\rho_0^{(i)}(\mathbf{r},\mathbf{r}')$ and isovector $\rho_1^{(i)}(\mathbf{r},\mathbf{r}')$ components of the density matrix:

$$\rho_0^{(i)}(\mathbf{r},\mathbf{r}')=\rho_n^{(i)}(\mathbf{r},\mathbf{r}')+\rho_p^{(i)}(\mathbf{r},\mathbf{r}'), \tag{9}$$

$$\rho_1^{(i)}(\mathbf{r},\mathbf{r}')=\rho_n^{(i)}(\mathbf{r},\mathbf{r}')-\rho_p^{(i)}(\mathbf{r},\mathbf{r}'), \tag{10}$$

where $\rho_p^{(i)}(\mathbf{r},\mathbf{r}')$ and $\rho_n^{(i)}(\mathbf{r},\mathbf{r}')$ are, respectively, the proton and neutron components of the density matrices of the colliding nuclei. Substituting (7)–(10) into (5), expanding all the functions in multipoles, and making a Fourier transformation, for the spherically symmetric part of the exchange potential we find

$$U^E(R)=4\pi\int_0^\infty \sum_{\tau=0,1} G_\tau(R,s)V_\tau^E(s)j_0(k(R)s/\eta)s^2ds, \tag{11}$$

$$G_\tau(R,s)=\frac{1}{2\pi^2}\int_0^\infty f_\tau^{(1)}(t,s)f_\tau^{(2)}(t,s)j_0(tR)t^2dt, \tag{12}$$

$$f_\tau^{(i)}(t,s)=4\pi\int_0^\infty \rho_\tau^{(i)}(\mathbf{r})\hat{j}(k_{\text{eff}}^{(i)}(\mathbf{r})s)j_0(tr)r^2dr. \tag{13}$$

In Eq. (11) the summation over $\tau$ implies summation over the isoscalar ($\tau=0$) and isovector ($\tau=1$) channels, $V_0^E$ and $V_1^E$ are, respectively, the isoscalar and isovector exchange components of the effective interaction, and $j_0(x)$ is the spherical Bessel function.

Equations (11)–(13) form the starting point for the calculation of the contribution of one-nucleon exchange effects to the potential in both the isoscalar and the isovector channels. Let us isolate the isovector part of the full interaction potential. Taking the isovector component $U_1^D(\mathbf{R})$ and the corresponding term with $\tau=1$ from Eq. (11), we obtain

$$U_1(R)=\int\int \rho_1^{(1)}(\mathbf{r}_1)V_1^D(s)\rho_1^{(2)}(\mathbf{r}_2)d\mathbf{r}_1d\mathbf{r}_2 + 4\pi\int_0^\infty G_1(R,s)V_1^E(s)j_0(k(R)s/\eta)s^2ds, \tag{14}$$

where $G_1(R,S)$ is given by (12) for $\tau=1$. In Eq. (14) the first term can be viewed as the generalization of the known expression from the folding model to the case of different neutron and proton distributions in the nucleus:[39]

$$U_1(R)=T_{z1}T_{z2}/A_1A_2\cdot\int\int \rho^{(1)}(\mathbf{r}_1)V_1^D(s)\times\rho^{(2)}(\mathbf{r}_2)d\mathbf{r}_1d\mathbf{r}_2, \tag{15}$$

where $T_{z1}$ and $T_{z2}$ are the values of the third projection of the isotopic-spin vector of the colliding nuclei. For protons or neutrons interacting with a nucleus, Eq. (15) gives the isobaric-spin potential of the Lane model.[40] The second term in (14) represents the contribution of one-nucleon exchange effects. The nucleon isobaric-spin potential has been studied by several authors (see, for example, Refs. 41 and 42) using the density-matrix formalism. The isospin–isospin potential for the interaction of composite particles explicitly including nucleon–nucleon exchange correlations was first constructed in Ref. 43 and was studied in detail in Ref. 44. Since the isovector potential is small compared with the isoscalar potential, it does not have as strong an effect on the elastic scattering cross section. However, it is necessary to include the isovector part of the potential in a comparative analysis of the elastic scattering of two isobars on the same target

nucleus with $N \neq Z$. This type of analysis has been performed for the elastic scattering of $^3$He and $t$ at low energies on the $^{14}$C target nucleus in Ref. 45. The part of the isospin–isospin interaction nondiagonal in the charge is responsible for charge-exchange transitions. In relation to this, it is interesting to study experimentally charge-exchange processes involving light nuclei with a neutron excess and to compare the corresponding angular distributions with the theoretical results. The first such studies have been carried out recently. Charge–exchange reactions were studied in Ref. 46 using an $^{11}$Li beam of energy 65 MeV/nucleon on $^1$H and $^2$H targets, and in Ref. 18 the angular distributions for excitation of the isobar-analog state in the reaction $^6$He$(p,n)^6$Li were measured. It was noted[18] that combined analysis of elastic scattering and charge–exchange reactions allows better determination of the neutron distribution in nuclei with a neutron excess.

Earlier, it had been shown (see, for example, Ref. 26) that the resulting potentials are more sensitive to the method of including one-nucleon exchange effects than to the form of the effective interaction. We shall use the complete M3Y interaction[47] based on the $G$-matrix elements of the Reid and Elliott interactions as the effective nucleon–nucleon interaction. For the isoscalar and isovector components of this interaction we have

$$V_0^D(s) = 7999\frac{\exp(-4s)}{4s} - 2134\frac{\exp(-2.5s)}{2.5s}, \tag{16}$$

$$V_0^E(s) = 4631\frac{\exp(-4s)}{4s} - 1787\frac{\exp(-2.5s)}{2.5s} - 7.847\frac{\exp(-0.7072s)}{0.7072s}, \tag{17}$$

$$V_1^D(s) = -4886\frac{\exp(-4s)}{4s} + 1176\frac{\exp(-2.5s)}{2.5s}, \tag{18}$$

$$V_1^E(s) = -1518\frac{\exp(-4s)}{4s} + 828.4\frac{\exp(-2.5s)}{2.5s} + 2.616\frac{\exp(-0.7072s)}{0.7072s}. \tag{19}$$

The scheme for constructing the real part of the optical potential presented in this section was used in Ref. 20 to analyze the quasielastic scattering of light exotic nuclei. The results of this analysis will be discussed in the second part of this review. A simplified version of this scheme is obtained by neglecting the second term in Eq. (3), but then it is usual to add a pseudopotential of zero range to the direct part of the effective forces.[48,49]

In another widely used version of the microscopic potential, only the first terms in Eq. (3) are kept, as before, but the DDM3Y interaction is used as the direct part of the effective nucleon–nucleon forces.[50,51] The quasielastic scattering of light exotic nuclei has recently been analyzed using an approach in which the DDM3Y effective interaction is used within the density-matrix formalism.[53]

In addition to the real part, the total optical potential must include the imaginary part responsible for absorption of the incident particle in inelastic channels. There are three basic methods of including the absorption potential in the microscopic optical model. In the first case the standard form of the imaginary part of the optical potential with Woods–Saxon radial dependence is used:

$$W^{(1)}(R) = W_{\mathrm{WS}}(R), \tag{20}$$

where the right-hand side can contain both a volume and a surface term [see Eq. (2)]. In this case the analysis of the experimental data requires many fitted parameters, which can introduce uncertainty in the results. Another approach is to choose the absorption potential to be proportional to the calculated real part:

$$W^{(2)}(R) = iN_W U(R), \tag{21}$$

where $N_W$ is the only fitted parameter in the absorption potential. However, Eq. (21) implies that the "geometry" of the real and imaginary parts of the potential is the same, which may not correspond to physical reality. It has therefore been proposed that the imaginary part of the optical potential be taken to be[20]

$$W^{(3)}(R) = i\left(N_W U(R) - \alpha R\frac{dU(R)}{dR}\right), \tag{22}$$

where $U(R)$ is the potential calculated in the microscopic approach. In Eq. (22), $N_W$ and $\alpha$ are parameters respectively characterizing the volume and surface parts of the absorption potential.

### 1.3. The polarization potential

Let us briefly discuss the basic methods of including the polarization addition to the potential [the real part of the second term in Eq. (1)]. This addition, which we denote by $\Delta U$, is small compared with the first term for nucleons at distances from the center of the nucleus for which the scattering cross section is sensitive to the optical potential.[49] This may not be true for composite projectiles. It was noted above that it is difficult to calculate $\Delta U$ in the entire volume using (1), but the contribution of individual processes to $\Delta U$ can be estimated. The calculation of the contribution of fragmentation $^{11}\mathrm{Li} \rightarrow {}^9\mathrm{Li} + 2n$ to $\Delta U$ is described in Ref. 4. The separability of the channel-coupling matrix elements and the WKB approximation were used in the calculation. Another variant of estimating $\Delta U$ using Eq. (1) is given in Ref. 54.

If the left-hand side of (1), i.e., the total optical potential, were known, $\Delta U$ could be represented as the difference

$$\Delta U = \mathrm{Re}\, V_{\mathrm{opt}} - \langle \phi_0 | V | \phi_0 \rangle. \tag{23}$$

The second term on the right-hand side of (23) is defined in the discussion of Eq. (1). In some studies $\Delta U$ was calculated from this expression, and the potential calculated in the Glauber approximation was taken for $\mathrm{Re}\, V_{\mathrm{opt}}$ (see, for example, Ref. 55). An ideologically similar method of finding $\Delta U$ was used in Ref. 56, where a term $\Delta U$, determined by the spline procedure from comparison of the theoretical and experimental angular distributions, was added to the calculated folding potential.

There are various phenomenological approaches for calculating $\Delta U$. The simplest is to renormalize the microscopic potential calculated using (1), i.e.,

$$U(R)+\Delta U(R)=N_v U(R). \tag{24}$$

Depending on the specific system and the energy considered, $N_v$ can be either larger or smaller than 1. This means that the polarization potential can be either repulsive or attractive. However, $\Delta U$ cannot always be included using Eq. (24), because the radial dependence of the second term in (1) can differ from that of the folding potential. Another method of phenomenologically including $\Delta U$ is to assume that $\Delta U(R)$ is proportional to the derivative of the Woods–Saxon form factor.[57] Yet another method is to use the representation[45,58]

$$\Delta U(R,E)=\alpha(E)W_v(R,E)+\beta(E)W_s(R,E), \tag{25}$$

where $\alpha$ and $\beta$ are free parameters.

### 1.4. The eikonal approximation and the Glauber theory

For a long time, nuclear scattering at intermediate energies was analyzed using the eikonal approximation and the Glauber theory.[21,59] As experimental data on reactions involving radioactive beams became available, these approaches have come to be used for analyzing the interaction of light exotic nuclei with stable targets, and also experiments with inverse kinematics. The Glauber theory was first used in Ref. 60 to analyze the total cross sections for the interaction of $^{11}$Li at 790 MeV/nucleon with various target nuclei. It was concluded that an extended neutron density tail exists in $^{11}$Li. In Ref. 61 the Glauber approximation was used to analyze charge-exchange reactions, and in Ref. 62 the elastic scattering of light exotic nuclei was studied. A four-body approach combined with the Glauber theory was developed in Ref. 63, and in Ref. 64 a lower limit of 30 MeV/nucleon was established for the validity of the Glauber approximation.

Let us briefly consider the formalism of the eikonal approximation and the Glauber theory. The standard expressions for the cross section and for the scattering amplitude (see, for example, Ref. 4) in the eikonal approximation have the form

$$\frac{d\sigma_{\rm el}}{d\Omega}=|F(\Theta)|^2, \tag{26}$$

$$F(\Theta)=f_c(\Theta)+ik\int_0^\infty bj_0(qb)\exp(i\chi_c(b))\times(1-\exp(i\chi_0(b)))db, \tag{27}$$

$$q=2k\sin(\Theta/2). \tag{27a}$$

Here $f_c(\Theta)$ is the Coulomb scattering amplitude, $k$ is the momentum of the relative motion, $j_0(x)$ is the Bessel function, the integration in (27) runs over the impact parameter $b$, and $\chi_c(b)$ and $\chi_0(b)$ are, respectively, the eikonal Coulomb and nuclear phase shifts:

$$\chi_0(b)=-\frac{1}{\pi v}\int_{-\infty}^{+\infty}U(\sqrt{b^2+z^2})dz, \tag{28}$$

$$\chi_c(b)=\frac{2Z_1Z_2e^2}{\pi v}\ln(kb). \tag{29}$$

In the case of intermediate energies the nuclear potential $U$ can be expressed in terms of the two-particle nucleon–nucleon transition matrix (the $t$ matrix). For nucleon–nucleus and nucleus–nucleus scattering we have

$$U_{NA}(R)=\langle t_{pn}\rangle\rho_n(R)+\langle t_{pp}\rangle\rho_p(R), \tag{30}$$

$$U_{A_1A_2}(\mathbf{R})=\int\langle t_{NN}\rangle\rho_1(\mathbf{R}-\mathbf{r}')\rho_2(\mathbf{r}')d\mathbf{r}'. \tag{31}$$

The averaged $t$ matrix is usually parameterized in terms of the nucleon–nucleon scattering cross section. Since the potentials explicitly involve the matter density distributions in the colliding nuclei, it becomes possible to extract information about the matter distribution by using this formalism to analyze elastic scattering.

Another approach to the use of Eqs. (26) and (27) is, instead of introducing the nuclear potential explicitly, to express the eikonal phase shift in terms of the profile function[4] $\gamma_{NN}$, which is the Fourier transform of the nucleon–nucleon scattering amplitude:

$$\gamma_{NN}=\frac{1}{2\pi ik_{NN}}\int\exp(-i\mathbf{qb})f_{NN}(\mathbf{q})d\mathbf{q}. \tag{32}$$

Use of the expansions of multiple scattering theory leads to the well known expressions for the scattering amplitude in the Glauber theory. For the nucleon–nucleus scattering amplitude we find

$$F_{NA}(\mathbf{q})=\frac{ik}{2\pi}\int\exp i\mathbf{qb}\left(1-\prod_{j=1}^{A}(1-\gamma(\mathbf{b}-\mathbf{s}_j))\right)|\Psi_A|^2d^2bd\mathbf{r}_1\ldots d\mathbf{r}_A. \tag{33}$$

Here $\gamma(\mathbf{b})$ is the profile function, and $\Psi_A$ is the wave function of the target nucleus in the ground state. The nucleus–nucleus scattering amplitude is a generalization of Eq. (33):

$$F_{AB}(\mathbf{q})=\frac{ik}{2\pi}\int\exp i\mathbf{qb}\left(1-\prod_{j=1}^{A}\prod_{n=1}^{B}(1-\gamma(\mathbf{b}-\mathbf{s}_j+\boldsymbol{\tau}_n))\right)|\Psi_A|^2|\Psi_B|^2d^2bd\mathbf{r}_1\ldots d\mathbf{r}_Ad\mathbf{t}_1\ldots d\mathbf{t}_B. \tag{34}$$

Here $\Psi_A$ and $\Psi_B$ are the wave functions of the ground state of the colliding nuclei. The calculation of the elastic scattering cross sections using Eqs. (33) and (34) directly is difficult. The various approximations used for Eqs. (33) and (34) are analyzed in Ref. 65. Results of evaluating the multiple integrals of the Glauber theory by the Monte Carlo method are also presented there.

### 1.5. Inclusion of inelastic scattering

The standard method of describing inelastic scattering in the case where elastic scattering is analyzed in the macroscopic optical model is to use the following expression as the form factor of the inelastic transition:[19]

$$F(R)=\beta_\lambda R_R V \frac{df_R(R)}{dR}+i\beta_\lambda R_I W \frac{df_I(R)}{dR}. \tag{35}$$

The deformation lengths of the real and imaginary potentials are taken to be identical:

$$\beta_\lambda R_R=\beta_\lambda R_I. \tag{36}$$

In Eq. (35), $f_i(R)$ $(i=R,I)$ is the usual Woods–Saxon radial form factor, and $\lambda$ is the angular-momentum transfer. Using the distorted-wave Born approximation or the coupled-channel method, the cross section for inelastic scattering can be calculated using the form factor $F(R)$.

If elastic scattering is analyzed in the microscopic optical model, it is natural to use derivatives of the microscopic optical potential in (35) instead of derivatives of phenomenological potentials. A more systematic approach is one in which the form factors for inelastic transitions are constructed using the transition densities and effective forces, taking into account nucleon–nucleon exchange correlations in the density-matrix formalism.[36] In this case not only is the description of elastic and inelastic scattering consistent, but also it becomes possible to verify the transition densities constructed in microscopic nuclear-structure models by analyzing inelastic scattering. This is especially important for light exotic nuclei in connection with the prediction that they have a soft excitation mode (for example, for $^{11}$Li).[66]

### 1.6. The nucleon densities

The analysis of quasielastic scattering requires the nucleon density distributions in the ground states of the colliding nuclei and the transition form factors, especially for low-lying collective states, which can play an important role via channel-coupling effects. For this it would be best to use the data of other experiments. For example, the proton distributions can be extracted with good accuracy from electron scattering. However, such data are available only for a limited number of stable nuclei. As far as the neutron densities are concerned, there are no data at all for them which are close in accuracy to the proton data. It is therefore necessary to use theoretical models. For light exotic nuclei, in which cluster degrees of freedom and effects of nearness to three-particle thresholds are important, it is usual to use models based on the explicit isolation of several principal clusters with the introduction of an effective interaction between them, taken from independent experiments. For example, in the case of $^6$He viewed as a three-body system $\alpha+n+n$, the $\alpha-n$ and $n-n$ interactions are introduced, and then the Schrödinger equation is solved by the Faddeev method, expansion in $K$ harmonics, the variational method, and so on.[67] The difficulties of this approach are associated with the approximate inclusion of the Pauli principle and the freezing of the clusters, the properties of which are assumed not to change in excitation or breakup of the system. In microscopic cluster models,[68,69] exchange effects arising from antisymmetrization of the total wave function are taken into account rigorously by calculating the corresponding matrix elements of the nucleon–nucleon interaction entering into the system Hamiltonian. The advantage of such models is that the same effective $N-N$ interaction can be used to attempt to reproduce the properties of individual clusters at large separations from each other (i.e., the properties of the ground and excited states of real nuclei, whose fusion can form the system in question) and the phase shifts of their scattering on each other, and to include cluster-rearrangement effects at small relative separations. In practical applications, the still insufficient computing power makes it important to restrict the number of basis configurations included in these models. This difficulty can to some degree be avoided by an approach recently proposed for solving the multinucleon Schrödinger equation, called the stochastic variational method.[70] It uses a correlated Gaussian basis and the method of trial and error for choosing the most important configurations, which prevents the "explosive" growth in dimension of the basis with increasing accuracy of the calculations. In self-consistent models of the mean-field type [the Hartree–Fock–Bogolyubov (HFB) method] the Pauli principle is rigorously satisfied, and rearrangement effects in going from one nucleus to another (for example, when the number of nucleons changes by 1–2 units, which is espe-

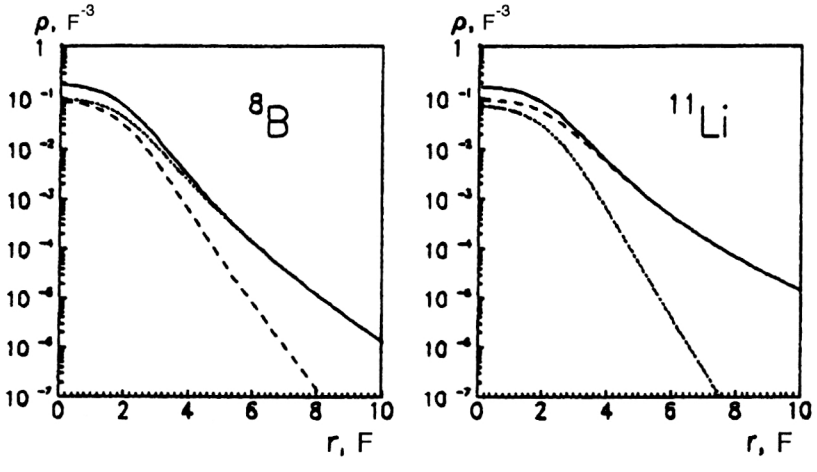


FIG. 1. Density distributions of neutrons (dashed lines), protons (dotted lines), and matter (solid lines) calculated using the density-functional method.[20]

cially important in light nuclei) are taken into account to a known degree. Here, strictly speaking, all the nucleons participate in forming the excited states described in the (quasiparticle) random-phase approximation (RPA), i.e., the nuclear system is "thawed out." However, this approach allows the description of only specific states (particle–hole, pair-vibrational), and not states of a cluster nature or three-particle dynamics, including complex decay channels. Nevertheless, in describing quasielastic scattering, when it is actually necessary to know only the ground-state densities, it is tempting to use the HFB method, because it allows the nucleon distributions for an arbitrary combination of colliding nuclei (except, of course, the lightest nuclei) to be obtained on a unified basis, with a single set of parameters. This approach was used in Ref. 20, and here we shall describe it in some detail.

The density-functional method was used in Ref. 20 on the basis of the Hohenberg–Kohn theorem[71] and the Kohn–Sham quasiparticle formalism,[72] which allows the introduction of a quasiparticle Hamiltonian with free kinetic-energy operator in which the effective nucleon mass $m^*$ coincides with the vacuum mass $m$ ($m^*/m=1$). The nucleon density $\rho$ is represented as a sum over filled one-particle orbitals, i.e., the shell sum minimizing the energy of the system. The quasiparticle spectrum and wave functions are calculated in the self-consistent mean field, which is the first functional derivative of the total energy with respect to the corresponding density, and the effective interaction is found as the second functional derivative. This approach can be viewed as a version of the self-consistent theory of finite Fermi systems,[73–75] which has much in common with the HFB method based on density-dependent effective forces.[76] The main problem is the choice of parametrization of the functional suitable for practical applications. One form was proposed in Ref. 22, where the $\rho$ dependence is introduced via linear-fractional functions, and surface effects are included via finite-range forces.

One of the sets of functional parameters used successfully for describing nuclear properties is given in Ref. 77. The neutron and proton density distributions and also their differences for lithium isotopes with mass number $A=6, 7, 8, 9, 11$, calculated using the density-functional method with the parameters of Ref. 77, were used in Ref. 44 to analyze the isoscalar and isovector optical potentials in the double-folding model with M3Y effective interaction in the scattering of lithium isotopes on various targets. The difference of the rms radii $\Delta r_{np}=\langle r_n\rangle^{1/2}-\langle r_p\rangle^{1/2}$ increases monotonically from nearly zero in $^6$Li to 0.52 F in $^9$Li, and then jumps sharply in $^{11}$Li, reaching 1.02 F, which indicates the appearance of a neutron halo. The behavior of the nucleon densities in $^{11}$Li is shown in Fig. 1, where we also show the distributions for the "exotic" nucleus $^8$B. They were obtained using the density-functional method with the same set of parameters. It is these densities that were used in Ref. 20 to analyze quasielastic scattering. The corresponding rms radii are given in Table I.

The value $\Delta r_{np}=1.02$ F for $^{11}$Li was obtained from these calculations, which confirms the presence of a long tail (neutron halo) in this nucleus. This has been seen both

TABLE I. Rms radii of several nuclei calculated using the density-functional method (F).

| Nucleus | $\langle r_n^2\rangle^{1/2}$ | $\langle r_p^2\rangle^{1/2}$ | $\langle r_m^2\rangle^{1/2}$ | $\Delta r_{np}$ |
|---|---|---|---|---|
| $^7$Be | 2.237 | 2.549 | 2.420 | −0.312 |
| $^8$B | 2.190 | 2.680 | 2.507 | −0.490 |
| $^{11}$Li | 3.255 | 2.235 | 3.011 | 1.020 |
| $^{11}$C | 2.326 | 2.456 | 2.398 | −0.130 |
| $^{12}$C | 2.387 | 2.406 | 2.396 | −0.019 |
| $^{28}$Si | 2.953 | 2.982 | 2.967 | −0.029 |

experimentally[60,78,79] and theoretically (for example, Refs. 67 and 80). Calculations using the HF method[80] gave the value $\langle r_m^2\rangle^{1/2}=2.846$ F, and for the charge radius $\langle r_{ch}^2\rangle^{1/2}=2.249$ F. Convolution of the point density distributions shown in Fig. 1 with the nucleon charge form factors gives the value $\langle r_{ch}^2\rangle^{1/2}=2.344$ F for the rms charge radius of $^{11}$Li. In three-dimensional cluster models, the method of Faddeev equations or hyperspherical harmonics gives the rms radius for $^{11}$Li in the range from 2.94 to 3.39 F, depending on the interaction used.[67] One can try to extract the values of the effective radius $\langle r_m^2\rangle^{1/2}$ and even the matter distributions themselves from experiment by analyzing the data on the total cross sections for reactions on various targets at various energies, using models of the Glauber type. In this way, the value $\langle r_m^2\rangle_{\rm exp}^{1/2}=3.10\pm0.17$ F was obtained for $^{11}$Li (Ref. 78), and the density profile shown in Fig. 2 was extracted in Ref. 79. The matter distribution for $^{11}$Li found using the density-functional method and shown in Fig. 1 is in good agreement with these results.

For the $^8$B nucleus the density-functional method gave $\Delta r_{np}=-0.49$ F, which is close to the value $-0.52$ F calculated using the cluster approach based on the resonating-group method in Ref. 69, and to the value $-0.42$ F obtained using the generator-coordinate method in Ref. 68. On the other hand, this value of $\Delta r_{np}$ is considerably larger in magnitude (by 50%) than the value found in Ref. 12, where it was concluded that there is no proton halo in $^8$B. As far as the experimental data for this nucleus are concerned, the first measurements at the Berkeley accelerator[78] obtained the "normal" value $\langle r_m^2\rangle^{1/2}=2.39\pm0.04$ F typical of $p$-shell nuclei, but the value 2.71 F was obtained from later measurements of the quadrupole moment.[5] The calculation using the density-functional method gives the intermediate value $\langle r_m^2\rangle^{1/2}=2.507$ F.

Finally, for $^7$Be the density-functional method gives $\Delta r_{np}=-0.31$ F, which is considerably smaller in absolute value than for $^8$B, but nevertheless suggests that this nucleus also has a proton skin. This value of $\Delta r_{np}$ for $^7$Be is also larger in absolute value than that in Ref. 12.

This discussion is illustrated in Fig. 1. The tail of the neutron distribution is expressed most clearly in the exotic $^{11}$Li nucleus, and also it is quite clear that the proton density in $^8$B significantly exceeds the neutron density for $r>3$ F. No features are observed in the "normal" nuclei $^{11,12}$C and $^{28}$Si. The charge radii for $^{12}$C (2.541 F) and $^{28}$Si (3.093 F) calculated with the same density functional are in reasonable agreement with the experimental values 2.471(6) and 3.086(18) F, respectively.[81]

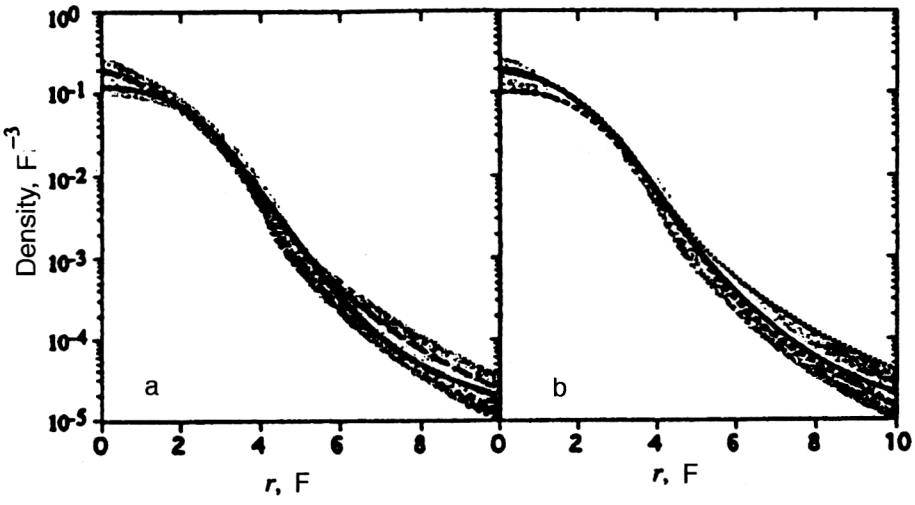


FIG. 2. Nucleon density distribution in $^{11}$Li extracted from experiments to measure the total interaction cross sections on various targets and at various energies.[79] The shaded region is the error corridor. The dashed and solid lines are obtained under the assumption that the neutrons of the halo are located in $1p$ and $2s$ orbitals, respectively. The dotted line is the calculation using the HF method[80] with neutron separation energy fitted to experiment.

## 2. ANALYSIS OF THE EXPERIMENTAL DATA

### 2.1. The angular distributions

#### *2.1.1. A general characteristic of the experimental scattering data*

As noted in the Introduction, two types of experiment have been carried out on the scattering of light exotic nuclei: scattering on compound nuclei (using, for example, $^{28}$Si and $^{12}$C as targets) and scattering of light exotic nuclei on protons in the inverse kinematical regime. Measurement of the angular distributions in reactions involving radioactive beams is very difficult experimentally. By now the angular distributions for the scattering of light exotic nuclei on compound targets have been obtained in an angular range of up to 20°, and the errors at large scattering angles are rather large. Moreover, the contribution of inelastic processes related to excitation of both the target nucleus and the projectile has not been isolated from the elastic scattering cross sections.

In the case of the scattering of light exotic nuclei on protons (experiments performed in the inverse kinematical regime), the angular range accessible to measurement is significantly larger, up to 65°. Here the cross sections for purely elastic scattering are measured, and in some cases the angular distributions are obtained for inelastic scattering with excitation of the projectile $^8$He (see Sec. 2.1.5).

#### *2.1.2.* $^{11}$Li+$^{28}$S *at* $E/A=29$ MeV/nucleon

The angular distributions of $^{11}$Li nuclei elastically scattered on a $^{28}$Si target at energy $E/A=29$ MeV/nucleon and also of $^7$Li at energy $E/A=25.4$ MeV have been measured in Ref. 9. In Fig. 3 we show the experimental data with the corresponding errors for the $^{11}$Li projectile. We see that in the given angular range the ratio $\sigma/\sigma_R$ for $^{11}$Li is nearly constant and close to unity, while for stable projectiles this ratio behaves diffractively and decreases rapidly in magnitude (see, for example, the experimental data for $^7$Li in Ref. 9).

The quasielastic scattering of $^{11}$Li on $^{28}$Si was analyzed using the optical model with phenomenological[9] and microscopic potentials.[9,20] In Table II we give the optical-potential parameters obtained from phenomenological analysis of the elastic scattering of $^7$Li and $^{11}$Li on $^{28}$Si. We see that two sets of reasonable parameter values are obtained for $^7$Li. However, it was not possible to find reasonable values for describing $^{11}$Li.

A more systematic approach to analyzing the quasielastic scattering of $^{11}$Li on $^{28}$Si is to construct microscopic optical potentials. This approach has been realized in Refs. 9 and 20. An approximate version of the microscopic approach was used in Ref. 9 to analyze the scattering of $^{11}$Li on $^{28}$Si. The microscopic potentials were calculated using the DDM3Y effective interaction without explicitly including one-nucleon exchange effects. The nuclear matter-density distributions were constructed using the standard Hartree–Fock scheme with Skyrme-2 effective forces.[76]

These experimental data were analyzed in Ref. 20. In Fig. 3 we show the results of calculating the scattering cross sections in the density-matrix formalism (see Sec. 1.2) using the neutron and proton densities constructed by the density-functional method (Fig. 1) and the absorption potential in the form (24). To test this theoretical approach, an analogous scheme was used to analyze the scattering in a system of two stable nuclei $^{12}$C+$^{12}$C at energy $E/A=20$ MeV/nucleon. It can be seen (see Fig. 3) that the description of the experimental data on the quasielastic scattering of $^{12}$C on $^{12}$C (Ref. 82) taking into account inelastic processes is quite good.

The qualitative description of the angular distributions for $^{11}$Li can be considered completely satisfactory: on the whole, the value of $\sigma/\sigma_R$ and the mildly sloping dependence of $\sigma/\sigma_R$ on the scattering angle are reproduced. As noted in Sec. 1.2, the densities of all nuclei, both projectiles and targets, are calculated using the same theoretical scheme. Since the curves shown in Fig. 3 correspond to the neutron and proton densities of $^{11}$Li, the integrated characteristics of which are given in Table I, it can be concluded that this microscopic analysis confirms the hypothesis that a neutron halo exists in $^{11}$Li.

The contribution of inelastic processes with excitation of the $2_1^+$ state in the $^{28}$Si target nucleus at $E_x=1.78$ MeV and in $^{12}$C at $E_x=4.44$ MeV (dashed lines in Fig. 3) was calculated using the inelastic form factor in the form (37) with the condition (38). The values of the deformation lengths were

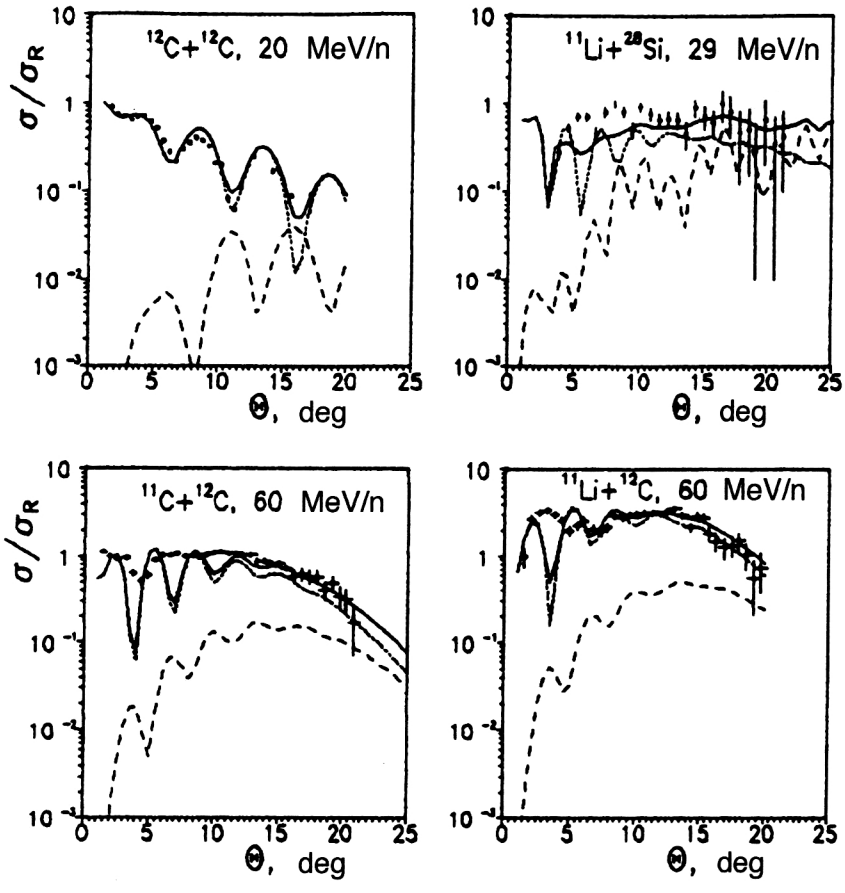


FIG. 3. Cross sections for quasielastic scattering of light nuclei. The experimental points are given with the errors, the solid line is the sum of the elastic and inelastic scattering cross sections, the dotted line is the elastic cross section, and the dashed line is the inelastic cross section.

chosen in accordance with the values of $B(E2)$ from Refs. 83 and 84 for $^{28}$Si and $^{12}$C, respectively. The angular distributions for elastic and inelastic scattering were calculated using a specially modified[20] version of the ECIS-88 program.[85] It can be seen that the contribution of inelastic processes is important only at large scattering angles and has practically no effect on the location and value of the first maxima and minima. The solid lines in Fig. 3 correspond to the incoherent sum of the elastic and inelastic scattering cross sections.

The analysis of the quasielastic scattering of $^{11}$Li on $^{28}$Si at energy $E/A=29$ MeV/nucleon leads to the following conclusions. The macroscopic optical model does not give a reasonable description of the experimental data if one uses the standard set of optical-potential parameters. Meanwhile, the two different microscopic approaches give equally good descriptions of the experimental angular distributions. Both microscopic descriptions confirm the hypothesis that a neutron halo exists in $^{11}$Li. However, the question of the disagreement between theory and experiment at scattering angles $\Theta=6°-10°$ remains open. In a recent study[86] another attempt was made to analyze microscopically the quasielastic scattering of $^{11}$Li on $^{28}$Si at $E/A=29$ MeV/nucleon, but no improvement in the description of experiment was obtained.

### 2.1.3. $^{11}$Li+$^{12}$C *and* $^{11}$C+$^{12}$C *at* $E/A=60$ MeV/nucleon

The quasielastic scattering of the isobars $^{11}$Li and $^{11}$C on $^{12}$C at energy $E/A=60$ MeV/nucleon was studied in Ref. 10. The experimental data together with their errors are shown in Fig. 3. The quality of the data is somewhat better than for the scattering of $^{11}$Li on $^{28}$Si. In contrast to that case, the ratio $\sigma/\sigma_R$ for the $^{12}$C target has a more pronounced structure at small scattering angles and decreases rapidly in absolute value beginning at the scattering angle $\Theta=14°$. Comparing the angular distributions for the $^{11}$Li and $^{11}$C isobars, it can be seen that the shapes of the angular distributions are different at small scattering angles ($\Theta\sim4°$), and that $\sigma/\sigma_R$ for $^{11}$Li is 2–3 times larger in magnitude than for $^{11}$C.

TABLE II. Parameters of the optical potentials and $\sigma_R$ for $^7$Li and $^{11}$Li interacting with a $^{28}$Si target.

| Projectile nucleus | $V_R$ | $r_R$ | $a_R$ | $W_v$ | $r_I$ | $a_I$ | $\langle r_R^2\rangle^{1/2}$ | $\langle r_I^2\rangle^{1/2}$ | $\sigma_R$ |
|---|---|---|---|---|---|---|---|---|---|
| $^7$Li | 226.75 | 1.286 | 0.853 | 37.26 | 1.739 | 0.809 | 4.38 | 5.08 | 1820 |
| $^7$Li | 114.2 | 1.286 | 0.853 | 29.75 | 1.739 | 0.809 | 4.38 | 5.08 | 1700 |
| $^{11}$Li | 204.48 | 0.585 | 1.737 | 8.23 | 2.18 | 0.425 | 6.604 | 5.36 | 1445.2 |

*Note:* In this and other tables where optical-potential parameters are given, $V$ and $W$ are in MeV, $r$ and $a$ in F, and the total reaction cross sections $\sigma_R$ in mb.

TABLE III. The same as in Table II, for $^{11}$C and $^{11}$Li interacting with a $^{12}$C target.

| Projectile nucleus | $^{11}$C | $^{11}$Li | | $^{11}$Li | |
|---|---|---|---|---|---|
| $N$ | 1 | 1 | | 2 | |
| $V_R$ | 40.0 | 40.0 | 40.0 | $V_{Rs}$ | 2.26 |
| $r_R$ | 0.990 | 0.810 | 1.015 | $r_{Rs}$ | 1.950 |
| $a_R$ | 0.981 | 1.907 | 1.055 | $a_{Rs}$ | 1.201 |
| $W_v$ | 25.92 | 25.09 | 20.73 | $W_s$ | 1.18 |
| $r_I$ | 0.986 | 1.226 | 1.077 | $r_{Is}$ | 1.646 |
| $a_I$ | 0.407 | 0.396 | 0.457 | $a_{Is}$ | 0.544 |
| $\sigma_R$ | 800.6 | 1180.8 | 1248. | | |

*Note:* See the footnote to Table II.

The quasielastic scattering of $^{11}$C and $^{11}$Li on $^{12}$C was analyzed according to various models: the macroscopic optical model,[87,88] the folding model,[10,20,53] and the Glauber and eikonal approximations.[63–65,89–91] In Table III we give the values of the optical-potential parameters obtained in Ref. 87 for the isobars $^{11}$C and $^{11}$Li scattered by the $^{12}$C target nucleus. The optimal (and far from satisfactory) description of the experimental angular distributions of $^{11}$Li using the standard optical model leads to an anomalously large (compared with $^{11}$C and other potential systematics) value of the diffuseness $a_R = 1.907$ F, whereas for the set from Table III the quasielastic scattering of $^{11}$C is described completely satisfactorily. Another attempt[87] to reproduce the experimental angular distributions of $^{11}$Li involved the introduction, into the real and imaginary parts of the potential, of surface terms whose parameters are given in the third line of Table III. The use of six additional parameters makes it possible to obtain a fairly good description of the quasielastic scattering cross section. However, the question of the meaning of these additional parameters arises. The conclusion of Ref. 87, that the scattering of $^{11}$Li on $^{12}$C at $E/A = 60$ MeV/nucleon indicates the presence of much stronger refraction than that seen in other heavy-ion scattering, is rejected in Ref. 92. In the latter study it is concluded that the results of Ref. 87 instead indicate that the scattering of $^{11}$C is more strongly refractive than that of $^{11}$Li. The best candidate for testing the refractive nature of the scattering process is scattering in the $^{16}$O+$^{16}$O system at 350 MeV (Ref. 93).

A standard macroscopic model for analyzing the scattering of $^{11}$C and $^{11}$Li on $^{12}$C was also used in Ref. 88. The values of the optical-potential parameters were taken to be the values of the potential for the $^{16}$O+$^{12}$C system. The description of the experimental data was not satisfactory, but the method of expansion of the elastic scattering amplitude proposed in Ref. 88 (see also Ref. 94) may be useful for analyzing the refractive properties of the potentials of light exotic nuclei.

A microscopic optical model for analyzing the scattering of the isobars $^{11}$C and $^{11}$Li on $^{12}$C at energy 60 MeV/nucleon was used in Refs. 10, 20, and 53. One-nucleon exchange effects were explicitly left out in constructing the microscopic potentials in Ref. 10, and the DDM3Y interaction was used as the effective interaction. The densities calculated in the Hartree–Fock method[80] were used for $^{11}$Li, and the shell-model densities were used for $^{11}$C and $^{12}$C. The optimal description of the experimental data required the introduction of renormalization constants for the real and imaginary parts of the potential: $N_v = 1.175$ and $N_w = 0.725$.

The results of calculating[20] the cross sections for quasielastic scattering using the scheme described in Sec.1.2 and above are shown in Fig. 3. It can be seen that the theoretical cross sections reproduce the experimental data for $^{11}$C, but have a more pronounced structure as a function of the scattering angle. In the case of $^{11}$Li this structure is manifested only at small scattering angles; in particular, the theoretical curve has a minimum at 4° and a maximum at 6°, which are not observed experimentally (the calculations in Ref. 10 lead to the same disagreement between theory and experiment). The values of the parameters $N_w$ and $\alpha$ obtained for the optimal description of the experimental data are identical for $^{11}$C and $^{11}$Li, i.e., $^{11}$C and $^{11}$Li are described with the same set of parameters in Ref. 20.

Yet another microscopic calculation for the systems $^{11}$Li+$^{12}$C and $^{11}$C+$^{12}$C was performed in Ref. 53. The experimental angular distributions were described just as well as in the microscopic analyses discussed above by varying two parameters $W_v$ and $r_I$ of the absorption potential and phenomenologically introducing [see Eq. (27)] polarization additions to the optical potential. A recent study[86] which used a microscopic version close to that described in Sec. 1.2 also analyzed these experimental data, but there was no improvement in their description.

The Glauber approximation has been used in a number of studies[63–65,89,90] to analyze the data on $^{11}$C and $^{11}$Li scattering on $^{12}$C. The first thorough analysis of the interaction of $^{11}$Li with $^{12}$C using the four-body model and the Glauber approximation was performed in Ref. 89. It was shown that $^{11}\text{Li} \rightarrow {}^{9}\text{Li} + n + n$ fragmentation processes play an important role in the interaction of $^{11}$Li with stable nuclei.

In Fig. 4 we show both the experimental data and the results of calculations[63] of the angular distributions of $^{11}$Li scattered on $^{11}$C at $E/A = 60$ MeV/nucleon in the Glauber approximation with $^{11}$Li densities constructed using various models. In Fig. 4a we give the results for purely elastic scattering, and in Fig. 4b we give the results for quasielastic scattering.

Let us remark on some important features of these results. It can be seen that when inelastic processes are not

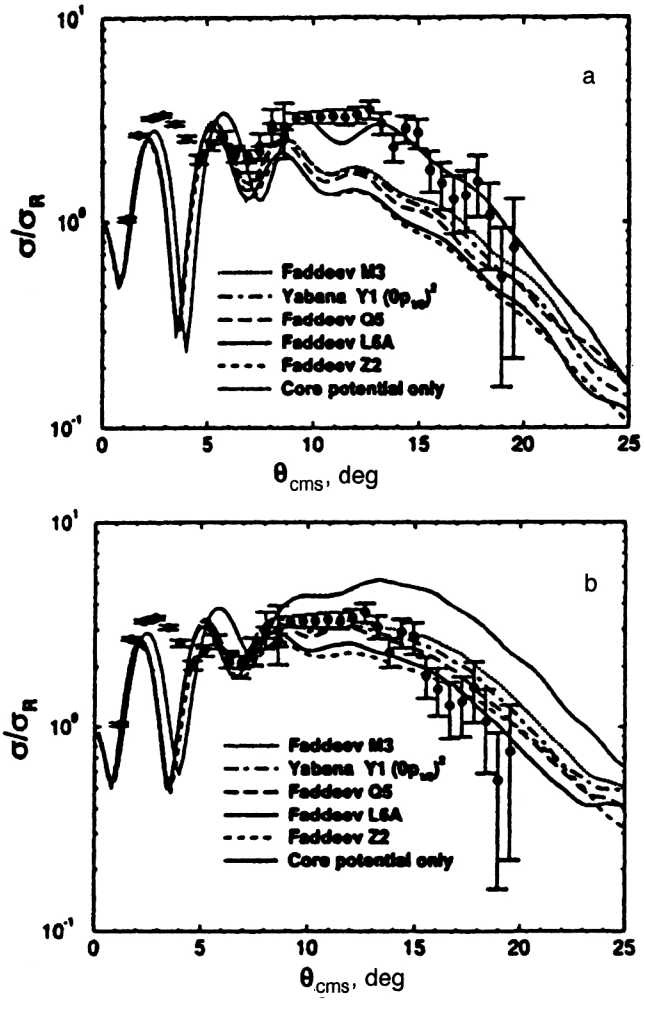


FIG. 4. (a) Cross sections for the elastic scattering of $^{11}$Li on $^{12}$C, calculated using various three-body models for $^{11}$Li and also only with the potential of the $^{9}$Li core. (b) The same as in (a) for quasielastic scattering.

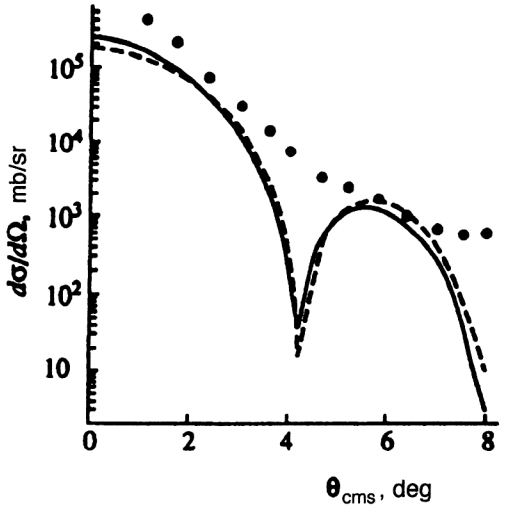


FIG. 5. Differential cross sections for $^{11}$Li+$^{12}$C and $^{12}$C+$^{12}$C elastic scattering at 60 MeV/$A$ (the solid and dashed lines, respectively). The points are the experimental data of Ref. 10 for $^{11}$Li+$^{12}$C.

included, all the theoretical curves lie below the experimental points, except in the version where the calculation includes only the core nucleons, i.e., $^{9}$Li, in $^{11}$Li. When inelastic processes are included, all the theoretical curves lie near the experimental points, and the cross section calculated by taking into account only the core nucleons is considerably larger than the experimental one for scattering angles larger than 10°. It can therefore be concluded that the nucleons of the halo play an important role in the correct description of the experimental data. The picture presented in Fig. 4 is also typical of the results of calculations using microscopic optical models. In Fig. 5 we show the cross sections for the elastic scattering of the isobars $^{11}$C and $^{11}$Li at $E/A=60$ MeV/nucleon on $^{12}$C calculated by the Monte Carlo method in Ref. 65. We see that the differences between the isobar cross sections are insignificant.

Let us discuss several studies in which the scattering of $^{11}$C and $^{11}$Li on $^{12}$C is analyzed using the Glauber or semiclassical approximation. The few-body model was used in Ref. 55 to construct a dynamical polarization potential on the basis of the Glauber approximation. It was shown that this potential is repulsive and therefore does not support the conclusion from the phenomenological analysis of Ref. 87 regarding the contribution of a long-range attractive part (see Table III). In Ref. 57, the scattering of $^{11}$C and $^{11}$Li on $^{12}$C was analyzed using the semiclassical approximation with a polarization potential introduced phenomenologically. It was concluded that in $^{11}$Li scattering the refractive properties of the potential are not manifested more strongly than in $^{11}$C scattering.

The four-body model in the Glauber approximation was used to analyze $^{11}$C and $^{11}$Li scattering in Refs. 64 and 90. It was shown that the breakup process $^{11}\text{Li}\rightarrow{}^{9}\text{Li}+n+n$ significantly affects the elastic scattering cross section. The most important part of the dynamical polarization potential is the absorption potential, and the addition to the real part is repulsive with large radius.[89] Several experimental situations, including the quasielastic scattering of $^{11}$Li on $^{12}$C at $E/A=60$ MeV/nucleon, were analyzed in the eikonal approximation in Ref. 91. When inelastic processes are included, the description of the experimental data is as good as in other studies.

Let us summarize our conclusions. As in the case of $^{11}$Li scattering on $^{28}$Si, the standard macroscopic optical model does not describe $^{11}$Li scattering on $^{12}$C for reasonable values of the optical-potential parameters. The various microscopic approaches (the folding model, the eikonal approximation, the Glauber theory) give roughly the same, completely satisfactory, qualitative description of the experimental angular distributions. However, all the theoretical calculations give a minimum at $\Theta=4°$ and a maximum at $\Theta=6°$, which are not observed experimentally. It has not been possible to determine the reason for this disagreement. The analysis performed in Ref. 20 is consistent with the hypothesis that a neutron halo exists in $^{11}$Li.

### 2.1.4. $^{9}$Li+$p$ at $E/A=60$ MeV/nucleon and $^{11}$Li+$p$ at $E/A=62$ MeV/nucleon

The elastic scattering of $^{9}$Li and $^{11}$Li nuclei on protons at the energies $E/A=60$ MeV/nucleon and 62 MeV/nucleon,

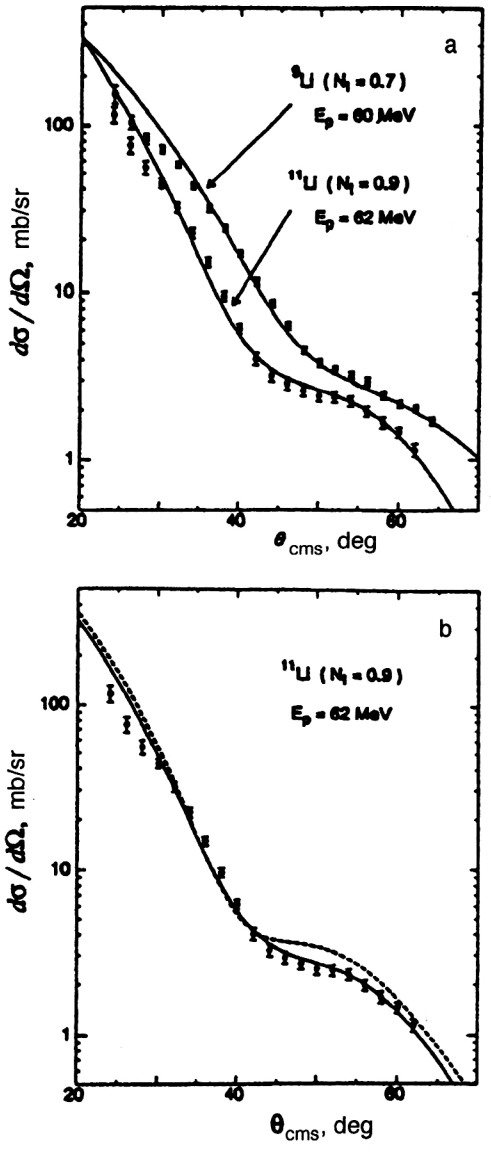


FIG. 6. (a) Angular distributions for $^9$Li and $^{11}$Li scattering on protons at energies of 60 and 62 MeV, respectively. The renormalization factor is $N_I = 0.7$ for $^9$Li and 0.9 for $^{11}$Li. (b) Dependence of the calculated angular distributions on the structure of the $^{11}$Li wave function. The dashed line corresponds to the wave function with smaller rms radius.

respectively, has been studied in Refs. 13 and 95. The experimental data are given together with the errors in Fig. 6. They cover the angular range from 25° to 65°. The relatively small measurement errors (compared with the case of $^{11}$Li scattering on $^{12}$C and $^{28}$Si) should be noted. Another advantage of experiments with inverse kinematics is that, in contrast to scattering on complex nuclei, the angular distributions of purely elastic scattering are measured. Comparing the results for $^9$Li and $^{11}$Li, two features of the scattering cross section for $^{11}$Li can be noted: first, the diffraction minimum is shifted to smaller angles than for $^9$Li ($\Theta_{min} \sim 44°$) and, second, the cross section is smaller than that for $^9$Li in the entire range of scattering angles accessible to measurement.

As in the case of $^{11}$Li scattering on complex nuclei, these experimental data were analyzed using various models: the

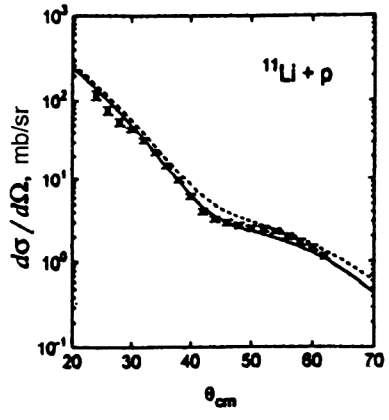


FIG. 7. Angular distributions of $^{11}$Li–$p$ elastic scattering calculated with (solid line) and without (dashed line) the polarization term.

standard optical model,[13,95,96] the microscopic optical model,[54,97,98] and the Glauber and eikonal approximations.[91,99,100] The angular distributions for the elastic scattering of Li isotopes were analyzed using the macroscopic optical model in Ref. 13. Here the optimal description of the experimental data for $^6$Li, $^7$Li, and $^9$Li required only an insignificant change of the parameters of the imaginary part of the optical potentials belonging to the global systematics.[101] Meanwhile, for $^{11}$Li some of the parameters ($r_R$, $a_R$, $r_I$, and $a_I$) essentially drop out of the set of systematics. Therefore, as in the case of $^{11}$Li scattering on complex targets ($^{12}$C and $^{28}$Si), all the geometrical parameters take values far from the standard ones.

A microscopic analysis of proton scattering on Li isotopes was carried out in Ref. 97. Here the real and imaginary parts of the optical potential were constructed using the local-density approximation of nuclear-matter theory,[52,102,103] and the parameter $N_I$, the renormalization of the strength of the absorption potential, was introduced to describe the experimental data. The results of the analysis are given in Fig. 6. It can be seen that for the parameter $N_I$ equal to 0.7 and 0.9 for the isotopes $^9$Li and $^{11}$Li, respectively, it is possible to describe successfully the experimental data, except for the region of small scattering angles for $^{11}$Li. An interesting result is presented in Fig. 6b. The solid line corresponds to the calculation with effective forces leading to the value $\langle r^2 \rangle_\rho^{1/2} = 3.24$ F, while the dashed line corresponds to $\langle r^2 \rangle_\rho^{1/2} = 2.82$ F. Therefore, the 15% change in the value of $\langle r^2 \rangle_\rho^{1/2}$ for $^{11}$Li, used as an input parameter in the microscopic analysis, significantly improves the description of the experimental angular distributions. This calculation confirms the existence of a neutron halo in $^{11}$Li. The problem of the disagreement between theory and experiment at small scattering angle remains for both $^9$Li and $^{11}$Li. A similar conclusion was drawn in Ref. 98, where a microscopic analysis of elastic scattering of $^{11}$Li on protons showed that the optimal description of the experimental data is obtained by assuming that $R_m = 3.20$ F for $^{11}$Li.

The role of the nucleons forming the halo in $^{11}$Li is illustrated in Fig. 7, where we present the results of the calculation from Ref. 54 with (solid line) and without (dashed line) the polarization term in the potential due to the valence

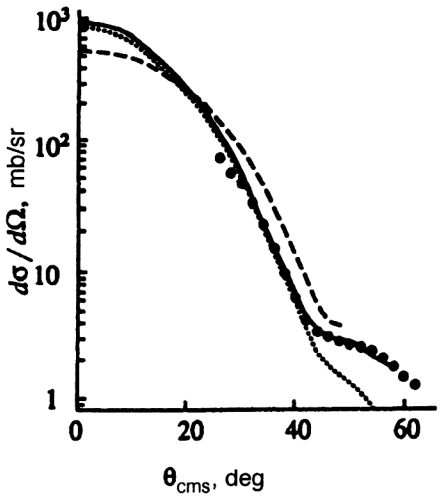


FIG. 8. Differential cross sections of $^{11}$Li+$p$ and $^{12}$C+$p$ elastic scattering at energy 60 MeV/nucleon. The points are the experimental data of Ref. 10 for $^{11}$Li+$p$, the solid and dashed lines are the calculations in the Glauber approximation for $^{11}$Li and $^{12}$C, and the dotted line is the calculation using the folding model.

nucleons in $^{11}$Li. The results of another microscopic calculation[65] are shown in Fig. 8. The calculation using the Glauber approximation (solid line in Fig. 8) gives a good description of the experimental data except at small scattering angles, while the calculation using the simplified folding model (dotted line in Fig. 8) disagrees with experiment in a large angular range. Since the difference between the Glauber cross section and the cross section calculated using the folding model is related to the polarization potential, the role of this potential can be seen in Fig. 8.

The four-body model in the eikonal approximation was used to analyze proton elastic scattering on $^{11}$Li in Ref. 99. The $p+^{11}$Li system was treated as a four-body system ($^9$Li+$n$+$n$+$p$), and the interaction between $^9$Li and the proton was described by an optical potential with a set of parameters which give a good description of $^9$Li scattering at 60 MeV/nucleon on protons.[13] The proton–neutron interaction was parametrized as a Gaussian with the effective inclusion of exchange. The description of the experimental data is just as good as in the studies described above. One of the important results of Ref. 99 is the conclusion that the dynamical polarization potential due to the breakup process $^{11}\text{Li}\rightarrow{}^9\text{Li}+2n$ gives a repulsive contribution to the real part of the optical potential, as in the case of $^{11}$Li scattering on $^{12}$C (Ref. 90).

The eikonal approximation with optical potentials from Ref. 13 was used in Ref. 91 to obtain a good reproduction of the experimental angular distributions for the scattering of $^9$Li with energy 60 MeV/nucleon and $^{11}$Li with energy 62 MeV/nucleon on protons. However, significant discrepancies between theory and experiment, especially for the $^9$Li projectile, arise in the microscopic version of the eikonal approximation in the $tpp$ scheme.[91] The authors attribute these discrepancies to the difficulty of taking into account the surface and spin–orbit terms in the optical potential in the microscopic version of the Glauber theory.[91] New experimental data on $^{11}$Li scattering on protons were recently obtained.[15] The angular distributions of elastic scattering were measured at the energy $E/A=75$ MeV/nucleon. The analysis led the authors[15] to conclude that low-energy elastic scattering is not really an effective tool for studying the details of the nucleon halo.

Experiments using inverse kinematics offer good possibilities for studying the properties of the halo in $^{11}$Li. However, as in the case of $^{11}$Li scattering on complex nuclei, the standard optical model does not lead to reasonable values of the optical-potential parameters.

### 2.1.5. $^8$He+$p$ at $E/A=73$ MeV/nucleon

Another experiment using inverse kinematics was performed in Ref. 14 in order to study the elastic and inelastic scattering of $^8$He at energy $E/A=73$ MeV/nucleon on protons. The experimental data along with their errors are shown in Fig. 9. The angular distributions for elastic scattering were obtained in the angular range up to $\Theta=65°$, although at scattering angles $\Theta>55°$ the measurement errors

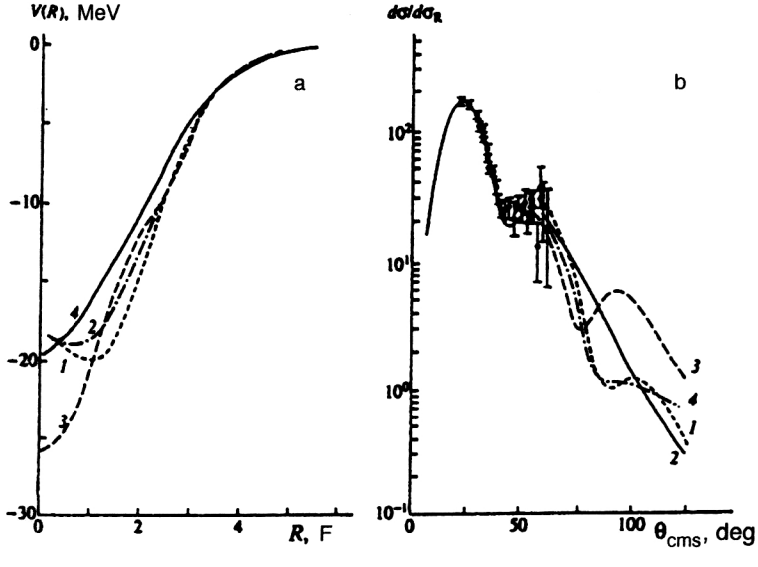


FIG. 9. Folding potentials (a) and the corresponding angular distributions (b) of $^8$He+$p$ elastic scattering at energy $E_{lab}=73$ MeV/nucleon relative to the Rutherford cross section, calculated for various density models, compared with the phenomenological real potential (curve *4*). The experimental data are from Ref. 14.

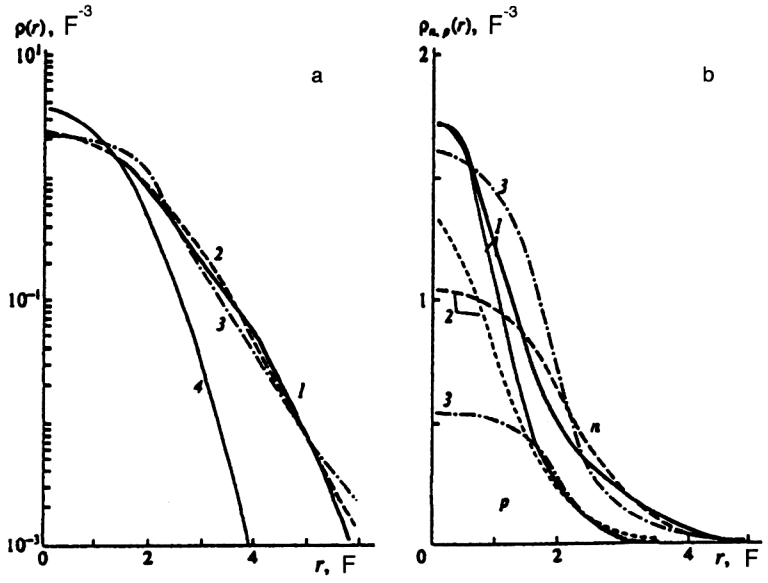


FIG. 10. Matter (a) and proton and neutron (b) densities of the $^8$He nucleus obtained in the COSM (curve *1*), DROP (2), and SW (3) models. In (a) we also show the density distribution of the $\alpha$ core in the COSM case (curve *4*). The notation for the curves in the same as in Fig. 9.

are quite large. In Ref. 104 the data were first analyzed using the standard optical model. Two sets of optical-potential parameters were used to describe simultaneously proton elastic and inelastic scattering on $^8$He. The curves for the angular distributions obtained using these potentials are close to each other and reproduce the experimental angular distributions well.[104] However, there are sizable differences in the values of a number of parameters, which indicates that it is impossible to extract unambiguous information about the potential from analysis of the experimental data according to the standard optical model.

The folding model with the M3Y interaction in the pseudopotential approximation for including one-nucleon exchange effects was used in Refs. 104 and 105 to analyze the experimental data on $^8$He scattering on protons. The main goal of the analysis was to check the sensitivity of the angular distributions to the matter density distributions in $^8$He calculated using various models. In Fig. 10 we show the matter, proton, and neutron densities of $^8$He obtained in the following models: COSM (the cluster–orbital shell model[106]), DROP (the drop model[107,108]), and SW (the Sorensen–Winther model[109]). Certain differences in the behavior of the densities in the surface region can be seen. The folding potentials calculated with these densities are shown in Fig. 9a, and in Fig. 9b we compare the angular distributions calculated using these potentials with the experimental angular distributions.

In Refs. 91 and 110 the scattering of $^8$He with energy $E/A=73$ MeV/nucleon on protons was analyzed using the eikonal approximation. The densities shown in Fig. 10 were used to calculate the cross sections in Ref. 110. The analysis showed that $\langle r^2\rangle_\rho^{1/2}$ for $^8$He agrees with the value obtained by studying fragmentation.[111] Models allowing a neutron skin in $^8$He give a better description of the experimental data, but the angular distributions are weakly sensitive (for the scattering angles accessible to measurement) to the shape of the matter distribution. Meanwhile, at higher energies the location of the diffraction minimum essentially depends on the matter distribution in the nucleus.

The $t\rho\rho$ scheme in the eikonal approximation was used in Ref. 91 to analyze $^8$He scattering on protons. The densities in $^8$He were calculated by the Hartree–Fock method, but a correction factor associated with the separation energy was introduced for the Hartree–Fock potential of the valence neutrons. These factors must be treated as additional free parameters. Using this scheme, it proved possible to obtain a satisfactory description of the experimental data on the elastic and inelastic scattering of $^8$He on protons.[91]

The angular distributions for the elastic scattering of $^8$He with energy 66 MeV/nucleon on protons were measured in Ref. 15. The eikonal approximation with $^8$He densities constructed in the cluster–orbital shell model gave a satisfactory description of experiment. In addition, the angular distributions for the elastic scattering of the isotope $^6$He on protons at $E/A=41.6$ MeV/nucleon were also recently measured.[18] The calculations carried out using both the macroscopic and the microscopic optical models gave values of the cross sections which are too high in relation to the experimental ones.[18]

Measurement of the angular distributions of $^8$He scattering on protons using inverse kinematics reveals new possibilities in the study of the properties of the exotic nucleus $^8$He. However, it is impossible to determine unambiguously the properties of the interaction potential using the standard optical model.

### 2.1.6. $^{12}$Be+$^{12}$C *and* $^{14}$Be+$^{12}$C *at* $E/A=56$ MeV/nucleon

The cross sections for the quasielastic scattering of $^{12}$Be and $^{14}$Be with energy $E/A=56$ MeV/nucleon on a $^{12}$C target were measured in Ref. 11. The data are shown in Fig. 11. The experimental errors, which are sizable, especially for large scattering angles, are not shown in the figure. The scattering cross sections have a weakly expressed structure and hardly decrease at all in the given angular range. The cross section for $^{12}$Be scattering is about twice as large as that for $^{14}$Be scattering. This fact is attributed[11] to the presence of a neutron halo in $^{14}$Be which leads to additional absorption. An

TABLE IV. The same as in Table II, for $^{12}$Be and $^{14}$Be interacting with a $^{12}$C target.

| Projectile nucleus | $^{12}$Be | | $^{14}$Be | | | $^{12}$Be | | $^{14}$Be | |
|---|---|---|---|---|---|---|---|---|---|
| $E$, MeV | 679.0 | | 796.0 | | | 679.0 | | 796.0 | |
| $N$ | 1 | 2 | 1 | 2 | | 1 | 2 | 1 | 2 |
| $V_R$ | 40.0 | 20.0 | 40.0 | 20.0 | $a_{Rs}$ | | 0.843 | 0.556 | 0.531 |
| $r_R$ | 0.990 | 0.924 | 0.838 | 0.702 | $W_s$ | 0.359 | 7.94 | 2.319 | 4.24 |
| $a_R$ | 0.932 | 2.466 | 0.694 | 0.560 | $r_{Is}$ | 1.753 | 1.046 | 1.806 | 1.323 |
| $W_v$ | 74.76 | 6.83 | 86.75 | 5.44 | $a_{Is}$ | 0.213 | 0.366 | 0.249 | 0.597 |
| $r_I$ | 1.003 | 0.683 | 1.003 | 0.762 | $\sigma_R$ | 1238. | 911. | 1900. | 1123. |
| $a_I$ | 0.497 | 1.261 | 0.716 | 0.146 | $\sigma_{2+}$ | 26.2 | 29.1 | 30.0 | 10.1 |
| $V_{Rs}$ | | 4.99 | 2.916 | 0.758 | $\sigma_{3-}$ | 4.0 | 10.8 | 10.3 | 4.1 |
| $r_{Rs}$ | | 1.115 | 1.954 | 1.817 | | | | | |

optical-model analysis of the experimental angular distributions was performed in Ref. 11 using potentials with the parameters given in Table IV (second and third columns). The description of the cross sections is satisfactory. The cross sections for inelastic scattering with excitation of $2^+$ and $3^-$ states in the target were calculated using the collective model (their values are also given in Table IV) and were incoherently added to the elastic scattering cross sections. The data in the table suggest that the optimal description of the experimental cross sections requires the introduction of a long-range surface term in the imaginary part of the optical potentials for both isotopes, while for $^{14}$Be a surface term should be introduced into the real part. The values of the total reaction cross sections obtained in this analysis are considerably larger than those obtained by extrapolation of the interaction cross sections measured at intermediate energies.[78]

The optical-model analysis of $^{12}$Be and $^{14}$Be scattering on $^{12}$C was reviewed in Ref. 112. The incoherent sum of the elastic scattering cross sections calculated using the potentials given in the fourth and fifth columns of Table IV and the inelastic scattering cross sections is shown by the solid lines in Fig. 11. On the whole, the description of the experimental data is slightly better than in Ref. 11. The total reaction cross sections $\sigma_R$ are, respectively, 911 and 1123 mb for $^{12}$Be and $^{14}$Be, and apparently are closer to the values which can be obtained by extrapolation. However, a number of the potential parameters from the fourth and fifth columns of Table IV differ strongly from the values obtained from the systematics for adjacent stable nuclei. Determination of the properties of the $^{12}$Be and $^{14}$Be potentials requires calculations in the microscopic approach. There has been one calculation in the eikonal approximation using the $tpp$ scheme for the cross sections for the quasielastic scattering of $^{12}$Be and $^{14}$Be on $^{12}$C (Ref. 91). However, it was not possible to obtain a satisfactory description of the experimental angular distributions. Therefore, at present the question of the interpretation of the experimental data shown in Fig. 11 remains open.

The angular distributions of the elastic scattering of $^{10}$Be and $^{11}$Be with energy 59.3 and 49.3 MeV/nucleon, respectively, on protons have been measured recently in an experiment using inverse kinematics.[18] The analysis was performed using macroscopic and microscopic models, but the calcu-

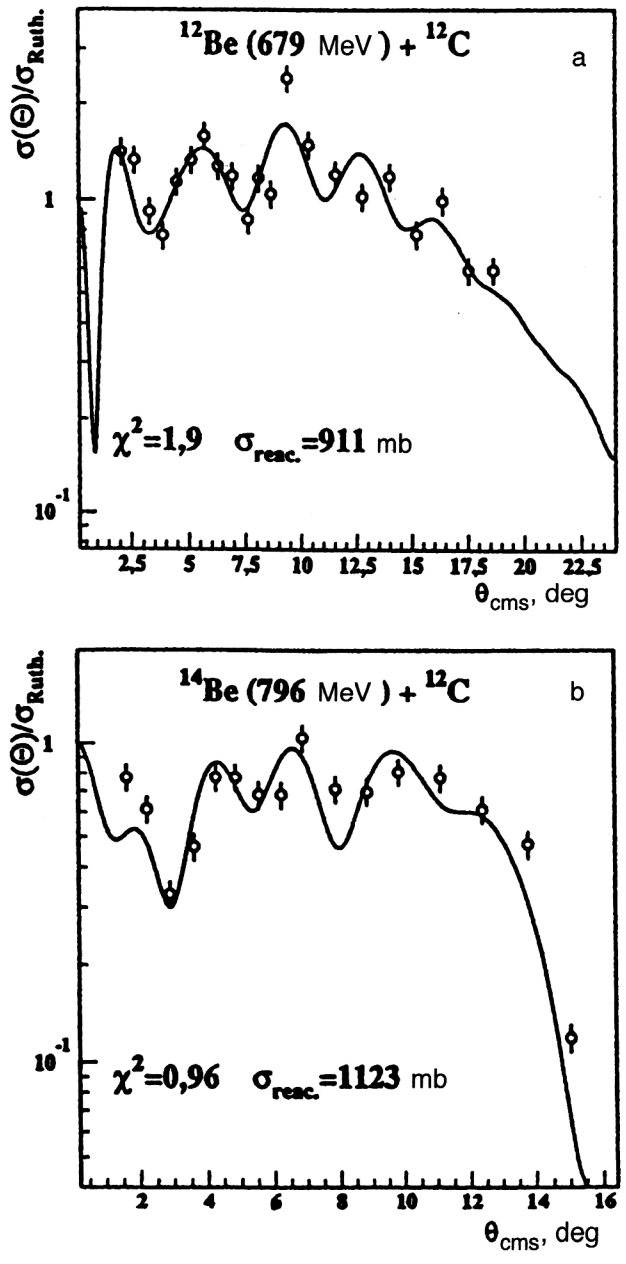


FIG. 11. (a) Experimental and theoretical angular distributions of $^{12}$Be quasielastic scattering on $^{12}$C. (b) The same as in (a) for $^{14}$Be.

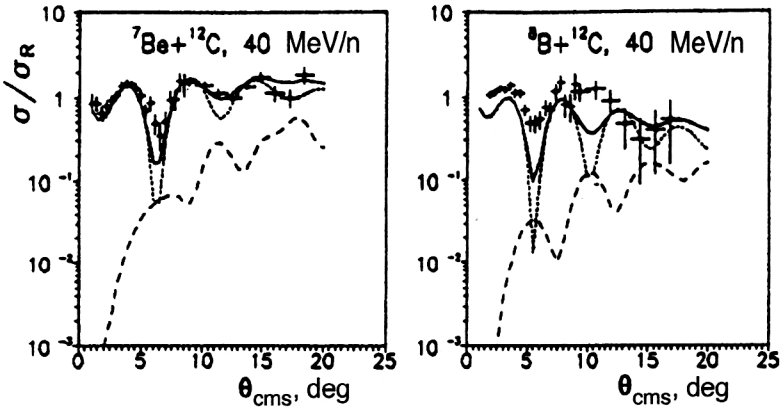


FIG. 12. Quasielastic scattering cross sections of light nuclei. The experimental points are given with the errors, the solid line is the sum of the elastic and inelastic scattering cross sections, the dotted line is the elastic cross section, and the dashed line is the inelastic cross section.

lated cross sections turned out to be too high in relation to the experimental ones.

### 2.1.7. $^8$B+$^{12}$C *and* $^7$Be+$^{12}$C *at* $E/A=40$ MeV/nucleon

As a result of the work in Ref. 5, the $^8$B nucleus with a proton excess became the first candidate for a nucleus with a proton halo. Accordingly, it is interesting to study the elastic scattering of $^8$B and also $^7$Be on a stable target nucleus. The cross sections for the quasielastic scattering of $^8$B and $^7$Be of energy $E/A=40$ MeV/nucleon on the $^{12}$C target nucleus were measured in Ref. 12 (the cross sections for $^7$Be scattering on $^{12}$C at 20 MeV/nucleon were obtained earlier[113]). The experimental data with their errors are shown in Fig. 12. It can be seen that the cross sections possess some structure as functions of the scattering angle. The cross section for the $^7$Be projectile almost does not decrease with increasing scattering angle, whereas for $^8$B the value of $\sigma/\sigma_R$ decreases by a factor of 3 to 4 in the same angular range.

A microscopic analysis of $^7$Be and $^8$B scattering on $^{12}$C was performed in Ref. 12. In that study one-nucleon exchange effects were not explicitly included, the effective forces from Ref. 52 were used, and various models were used to construct the projectile and target densities. To obtain an optimal description of the experimental cross sections, renormalization factors were introduced for both the imaginary and the real parts of the constructed potential. In Ref. 20 the experimental data were analyzed using the density-matrix formalism, with the neutron and proton densities calculated by the density-functional method.[114] The integrated characteristics of the corresponding distributions are given in Table I. In Fig. 12 we show the results of the microscopic calculation of the angular distributions with the values of the parameters $N_w$ and $\alpha$ given in Table V. The microscopic analysis performed in Ref. 20 suggests that the proton density has considerable extent in $^8$B and less in $^7$Be.

## 2.2. The total reaction cross sections

It was noted in the Introduction that a quantity sensitive to the properties of the potential, and, in the microscopic approach, to the integrated properties of the matter distribution in nuclei, is the total reaction cross section $\sigma_R$. Therefore, in order to limit the uncertainties associated with the magnitude of the potential, especially the absorption potential, it is necessary to perform a simultaneous analysis of the angular distributions and the total reaction cross sections and to have available the corresponding experimental data. Unfortunately, most of the data for $\sigma_R$ have been obtained at intermediate energies ($E/A=790$ MeV/nucleon). The interaction cross sections $\sigma_I$ rather than the total reaction cross

TABLE V. Total reaction cross sections (mb).

| Reaction ($E/A$) | Theory | Theory (Ref. 20) | Experiment |
|---|---|---|---|
| $^{11}$Li+$^{28}$Si (29 MeV/n) | 1402 (Ref. 9) | 1970 ($N_w=0.25$, $\alpha=0.03$) | 2947±386 (Ref. 115)[a] |
| $^{11}$Li+$^{12}$C (60 MeV/n) | 1350 (Ref. 10) | 1488 ($N_w=0.30$, $\alpha=0.05$) | ≈1600 (Ref. 89)[b]<br>1040±60 (Ref. 60)[c] |
| $^{11}$C+$^{12}$C (60 MeV/n) | - | 1280 ($N_w=0.30$, $\alpha=0.05$) | - |
| $^{12}$C+$^{12}$C (20 MeV/n) | 1453 (Ref. 117) | 1486 ($N_w=0.30$, $\alpha=0.03$) | ≈1370 (Ref. 118)[d] |
| $^7$Be+$^{12}$C (40 MeV/n) | 1026 (Ref. 12) | 1102 ($N_w=0.50$, $\alpha=0.$) | 738±9 (Ref. 60)[c] |
| $^8$B+$^{12}$C (40 MeV/n) | 1104 (Ref. 12) | 1201 ($N_w=0.30$, $\alpha=0.03$) | 784±14 (Ref. 78)[c] |

[a]Measured at 25.5 MeV/nucleon.
[b]Estimate from the systematics in Ref. 10.
[c]Interaction cross section measured at 790 MeV/nucleon.
[d]Estimate at 20 MeV/nucleon from the systematics.

sections $\sigma_R$ have been measured. There are differences between $\sigma_R$ and $\sigma_I$ owing to the contribution of inelastic scattering. These differences are estimated to be 5–10% at intermediate energies. At low energies $\sigma_R$ has been measured only in a few cases (see, for example, Refs. 115 and 116). For the other cases $\sigma_I$ is extrapolated to low energies. It should be remembered that the reaction cross sections depend strongly on energy,[116] and so the extrapolation procedure can involve large errors.

Let us consider some of the results for the total reaction cross sections obtained in microscopic approaches. In Table V we give the values of $\sigma_R$ calculated in the microscopic optical model[20] for all the experimental cases shown in Figs. 6 and 7; we also give the values of the parameters $\alpha$ and $N_w$ for which the optimal description of the experimental data is obtained, and the values of $\sigma_R$ calculated in other theoretical approaches. On the whole, it can be stated that the microscopic model developed in Ref. 20 gives a reasonable description of both the angular distributions and the total reaction cross sections, while it involves only two free parameters.

The angular distributions and $\sigma_R$ were also analyzed simultaneously for the system $^{11}$Li+$^{12}$C in Ref. 53. The value $\sigma_R = 1473$ mb (cf. Table V) was obtained by increasing the radius of the absorption potential by 10% and phenomenologically including polarization additions to the real and imaginary parts of the potential. A comparison between theory and experiment for $\sigma_R$ at two values of the energy, $E/A = 75$ and 87 MeV/nucleon, was also made in Ref. 53. However, the angular distributions of $^{11}$Li quasielastic scattering on $^{12}$C at these energies have not yet been measured. The values of the total reaction cross sections for the system $^{11}$Li+$^{12}$C at low and high energies are discussed in Ref. 8. It is pointed out that no single model describes $\sigma_R$ in the entire energy range.

The total reaction cross sections for the system $^{8}$B+$^{12}$C were measured at four values of the energy in Ref. 116. The values of $\sigma_R$ calculated in the Glauber approximation are in good agreement with the experimental values. However, the angular distributions of the quasielastic scattering of $^{8}$B on $^{12}$C were measured only at $E/A = 40$ MeV/nucleon. Good agreement between theory and experiment for $\sigma_R$ was also obtained in Ref. 119, and the effect of the parameters $N_w$ and $\alpha$ on $\sigma_R$ as well as the calculated angular distributions of $^{8}$B elastic scattering on $^{12}$C were analyzed in a wide energy range.

## 3. THE NUCLEON HALO AND THE SOFT MODE

The existence of nuclear states with unusually extended spatial distributions was already discussed 25 years ago[120,121] for systems with two resonantly interacting particles weakly coupled to a third body, the core. However, only recently did it become clear that a similar situation can occur in nuclei. For example, in $^{11}$Li with two weakly coupled neutrons above the $^{9}$Li core, a two-neutron halo was discovered with associated strong dipole excitations near the continuum threshold with anomalously small energy. This is called the dipole soft mode. Anomalously extended matter distributions and large probabilities for electromagnetic dissociation have also been discovered in other light nuclei (for example, in $^{11}$Be, which has a one-neutron halo). These results have been widely discussed in reviews (see, for example, Ref. 8). However, we note that so far there has been no experimental observation of other predicted[66,122] strong low-energy excitations in nuclei with small energy separation of the nucleons which form a packet of multipole transitions near the continuum threshold. Their appearance can be explained in terms of a very simple model of independent particles in a potential well.

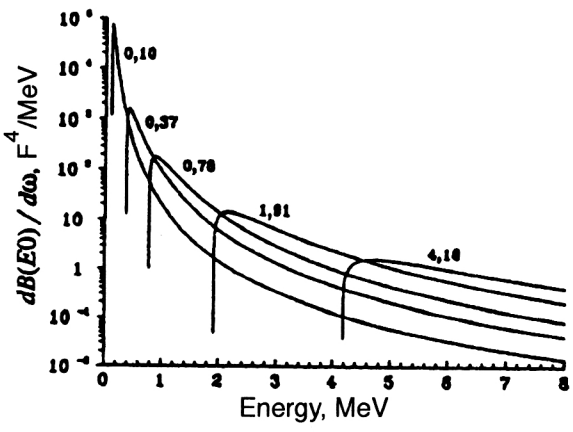


FIG. 13. Monopole response of the $1s$ neutron in a spherical square well of radius 2 F. The numbers on the curves indicate the binding energy of the neutron level.

Let us consider a $1s$ neutron in a spherical potential of square-well form with fixed radius $R$ and find the distribution of monopole transitions to the continuum in an external field $V_0 \propto r^2 Y_{00}$ as a function of the neutron binding energy by varying the well depth $U$. The transition-strength distribution is given by

$$\frac{dB(E0)}{d\omega} = \frac{1}{4\pi} \int y_\epsilon(r) r^2 y_\lambda(r) dr, \tag{37}$$

and the energy-weighted sum rule has the form

$$\int \omega \frac{dB(E0)}{d\omega} d\omega = \frac{\hbar^2}{2m} \frac{1}{\pi} \langle r^2 \rangle, \tag{38}$$

where $\langle r^2 \rangle = \int y_\lambda(r) r^2 y_\lambda(r) dr$, $y_\lambda(r)$ is the radial wave function of the bound neutron in the $\lambda = 1s$ level with binding energy $\epsilon_\lambda$, $y_\epsilon$ is the continuum wave function with energy $\epsilon$ normalized to $\delta(\epsilon - \epsilon')$, and $\omega = \epsilon + \epsilon_\lambda$ is the transition energy. For $r > R$ we have $y_\lambda(r) \sim \exp(-\kappa r)$, $y_\epsilon \sim \sin(pr + \delta_0)$, where $\kappa = \sqrt{2m\epsilon_\lambda}/\hbar$ and $p = \sqrt{2m\epsilon}/\hbar$. It is easily seen that for $\epsilon_\lambda \to 0$ the mean-square radius $\langle r^2 \rangle$ diverges, $\sim 1/\kappa^2$ (i.e., $\sim 1/\epsilon_\lambda$), and the situation of an "ideal" halo occurs, where the probability of finding the neutron outside the well tends to 1 (Ref. 7). Then, when we take the limit $\epsilon \to 0$, the leading divergent term in the differential monopole strength is $dB(E0)/d\omega \sim p\kappa/(p^2 + \kappa^2)^4$ [i.e., $\sim \delta(\omega)/\omega^2$]. As a result, for $\epsilon_\lambda \to 0$ the entire monopole-transition strength is concentrated at the continuum threshold. This conclusion is illustrated in Fig. 13, where we show the distributions of $dB(E0)/d\omega$ for the case of a well of radius $R = 2$ F. The first $s$ level in this well appears at

$U_{\min}=12.79$ MeV. By taking the well depth to be $U=U_{\min}+\Delta$ and varying $\Delta$ in the range from 12 to 1.5 MeV, the location of the neutron $s$ level can be shifted from 4.18 MeV to 100 MeV. We see from the figure that the mildly sloping distributions of the monopole strength beginning at the corresponding thresholds $\omega>\epsilon_\lambda$ are gradually replaced by a $\delta$-like peak near $\omega=0$. This is the monopole soft mode.

As the orbital angular momentum $l$ increases, the ideal halo does not appear, owing to the centrifugal barrier: already for a $p$ neutron the probability of finding it in the region $r>R$ for $\epsilon_\lambda\to 0$ is $\approx 60\%$, and for a $d$ neutron it is only $\approx 40\%$ (Ref. 7). In the case of protons, the situation for forming a halo is even more unfavorable, especially as the core charge $Ze$ increases. For example, even for an $s$ proton there is a 50% probability of finding it outside a core of the same radius $R$ as in the example above when its separation energy tends to zero only if $Z<8$.

However, these arguments do not mean that there is no structure in the excitation spectrum for nuclei with a weakly coupled valence shell. The fact that strong multipole transitions with low energy concentrated near the continuum threshold can arise in such nuclei can be demonstrated by using the same simple microscopic model of independent particles in a self-consistent finite potential by means of the sum rules.[66,123] This is a completely realistic model, because the excitations in question are separated by a large energy gap from the core excitations. In this model, for the multipole operator of the external field $V_0^{(L)}=r^L Y_{LM}$ the integrated sum of reduced transition probabilities is given by

$$m_0^{(L)}=\sum_s B(EL\uparrow;\omega_s)=\frac{2L+1}{4\pi}\langle r^{2L}\rangle A - \sum_{nlj,n'l'j'}(nlj\|V_0^{(L)}\|n'l'j')^2, \tag{39}$$

where the summation runs only over filled orbitals. The energy-weighted sum rule has the form

$$m_1^{(L)}=\sum_s \omega_s B(EL\uparrow;\omega_s)=\frac{\hbar^2}{2m}\frac{L(2L+1)^2}{4\pi}\langle r^{2L-2}\rangle A, \tag{40}$$

where $A$ is the number of particles, $\omega_s$ is the excitation energy, and the angle brackets $\langle\ldots\rangle$ denote the expectation value in the ground state. Now we can introduce the energy centroid of the excitations $\bar\omega^{(L)}$ in the field $V_0^{(L)}$:

$$\bar\omega^{(L)}=m_1^{(L)}/m_0^{(L)}. \tag{41}$$

For sufficiently large $L$ the second (two-particle) term in $m_0^{(L)}$ vanishes (for example, for $L\geqslant 3$ in $^{11}$Li). When the binding energy of the valence nucleons $\varepsilon_{\rm val}$ tends to threshold, the main contribution to the moments $m_{0,1}^{(L)}$ comes from the diagonal matrix element between the wave function $R_{\rm val}$ of these nucleons. Taking the case of neutrons for simplicity, we can easily estimate these moments for $\varepsilon_{\rm val}\to 0$, using the asymptote $R_{\rm val}(r)\propto\exp(-\kappa r)/r$, where $\kappa=\sqrt{2m\varepsilon_{\rm val}}/\hbar$. Then $\langle r^{2L}\rangle=(2L)!/(2\kappa)^{2L}$, and

$$\bar\omega^{(L)}=2\frac{2L+1}{2L-1}\varepsilon_{\rm val}. \tag{42}$$

For $^{11}$Li this expression is applicable for $L>0$. In the case $L=0$, for the field $V_0^{(0)}=r^2Y_{00}$, in the limit $\varepsilon_{\rm val}\to 0$, taking into account the diagonal matrix element in the two-particle term, we have

$$\bar\omega^{(0)}=8\varepsilon_{\rm val}/5. \tag{43}$$

This simple treatment shows that the centroid of the multipole strength distribution for all $L$ tends to zero energy when the valence level approaches the continuum, so that the total strength is localized at threshold. It also follows that for sufficiently large multipole orders $L\gg A^{1/3}$ the main contribution to the nuclear excitation probability will come from weakly bound nucleons, whose wave function has a longer tail, and in this case the transition strength will be concentrated at the same energy $\bar\omega\approx 2\varepsilon_s$, where $\varepsilon_s$ is the nucleon separation energy.[124,125] We also note that the width of such "exotic" multipole distributions must be of order $\varepsilon_{\rm val}$, because there are no other parameters with the dimensions of energy in the problem. Broader distributions should be expected for other operators containing, in particular, a dependence on the momentum transfer $q$ in the expansion of realistic external fields in Bessel functions $[V_0^{(L)}\propto j_L(qr)Y_{LM}]$ (Ref. 125). The dipole soft mode determines the probability for electromagnetic (Coulomb) dissociation of exotic nuclei, and the contribution of the other modes to this process is negligible. Unfortunately, so far there are no experimental possibilities for studying multipole soft modes with $L\neq 1$ in electromagnetic processes.

As was noted in Ref. 66, similar soft modes should appear in any nuclear model, because their existence arises only from the slow falloff of the valence-nucleon wave function at large distances, although asymptotically this falloff can differ from an exponential dependence. Calculations using cluster models[126,127] have confirmed this prediction. Similar peaks of soft transitions must also exist in other nuclei with a neutron excess near the drip line ($^6$He, $^8$He, $^{11,14}$Be). Since these transitions are responsible for a significant part of the sum rules, they are called giant resonances at the continuum threshold: a new soft mode. However, they are not resonances in the usual sense, but simply correspond to direct transitions to the continuum, and the time that they take is several orders of magnitude smaller than expected from the uncertainty principle.[128]

One can attempt to observe strong low-energy transitions in any nuclear inelastic scattering reaction, because they should be strongly excited both in isovector and in isoscalar external fields. In particular, as was shown in Ref. 123, the probability of exciting the monopole soft mode is large in forward scattering at small angles. As an example, inelastic proton scattering on $^{11}$Li was studied in Ref. 123. The calculations were performed for two incident proton energies, $E_p=60$ and 100 MeV, using the distorted-wave method with the assumption that the one-stage direct $(p,p')$ reaction mechanism dominates at small scattering angles. The optical potentials describing the relative nucleon–nucleus motion were taken from the systematics of data on elastic proton scattering on $^{12}$C (Ref. 129). The effective interaction between the incident proton and the target nucleons was taken to be the M3Y interaction[130] and the free $t$ matrix[131] at 60

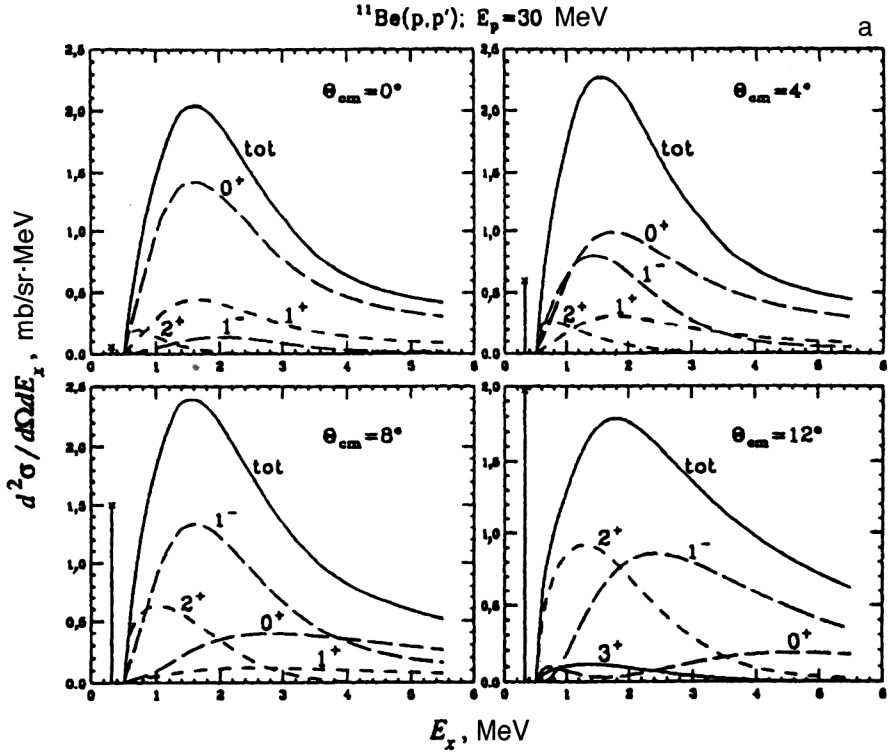


FIG. 14a. Inclusive energy spectra of protons from the reaction $^{11}$Be$(p,p')$ at $E_p=30$ MeV (a) and $\alpha$ particles from the reaction $^{11}$Be$(\alpha,\alpha')$ at $E_\alpha=120$ MeV (b) for four different scattering angles. The contributions from transitions from the one-neutron halo into the continuum with various transfers $J^\pi$ are shown. The vertical lines with the cross correspond to the cross sections (in mb/sr) for the transition between the ground $(1/2^+)$ and first excited $(1/2^-)$ states in $^{11}$Be.

and 100 MeV, respectively, taking into account the central, tensor, and spin–orbit components. Exchange effects were included in the pseudopotential approximation.

Another example of inelastic hadron scattering on the exotic $^{11}$Be nucleus, which has a one-neutron halo, has been studied by one of the coauthors of the present review (S.F.) and S. N. Ershov at Dubna. They studied the $^{11}$Be$(p,p')$ reaction at $E_p=30$ MeV and the $^{11}$Be$(\alpha,\alpha')$ reaction at $E_\alpha=120$ MeV. The cross sections of these reactions were calculated in the distorted-wave Born approximation with the optical potentials from Ref. 132 for $(p,p')$ and from Ref. 133 for $(\alpha,\alpha')$ and the M3Y effective nucleon–nucleon interaction. In the case of proton scattering the central, tensor, and spin–orbit components of the effective forces were included, while for $\alpha$-particle scattering the central and tensor ones were used. The transition densities were taken to have the form of products of one-particle wave functions in a self-consistent potential calculated using the density-functional method described above with additional variation of the depth in order to reproduce the neutron separation energy of 505 keV (from the $2s_{1/2}$ level) and the first excited bound state $(1p_{1/2})$ with energy 320 keV. The results of the calculation are shown in Fig. 14. We see that for scattering at zero angle these reactions are dominated by the process with excitation of the monopole soft mode, especially in the case of $\alpha$ particles. However, as the scattering angle increases other multipole soft transitions rapidly become important. Nevertheless, at all the angles studied the sum of these leads to a characteristic asymmetric maximum in the spectra of inelastically scattered particles.

The excitation of soft transitions in the inelastic scattering of $^{11}$Li on $^{12}$C at intermediate energies was also studied in Ref. 134, using the eikonal approximation with the microscopic HF-RPA transition densities. It was concluded that it is possible in principle to distinguish the contributions from monopole, dipole, and quadrupole transitions at small angles.

Thus, inelastic hadron scattering may prove to be a very useful tool for studying soft excitation modes in exotic nuclei with weakly bound nucleons. The rapid progress made in recent years in experimental techniques involving the use of radioactive beams and methods of measuring reaction products allows us to hope that in the very near future new soft modes will be discovered and studied in sufficient detail to check the predictions. These hopes are supported by the recent first experimental data on the spectroscopic study of $^{11}$Li inelastic scattering on protons at 75 MeV/nucleon (Ref. 15).

## CONCLUSION

The study of the quasielastic and elastic scattering of light exotic nuclei has become an important component of the investigation of the properties of nuclei far from the $\beta$-stability line. So far there have only been a few measurements of the angular distributions for the projectiles $^6$He, $^8$He, $^{11}$Li, $^7$Be, $^8$B, $^{12}$Be, and $^{14}$Be at energy $E/A$ ranging from 20 to 75 MeV/nucleon. The experimental conditions in studying scattering on a compound target ($^{12}$C, $^{28}$Si) have been such that the contribution of inelastic scattering processes with excitation of states of the target nucleus or the projectile is not separated from the elestic scattering cross sections, and the angular range accessible to measurement is limited to the scattering angle $\Theta=20°$. Experiments on the scattering of $^6$He, $^8$He, $^9$Li, $^{11}$Li, $^{10}$Be, and $^{11}$Be on protons have been carried out using inverse kinematics for a wide range of scattering angles and involve smaller

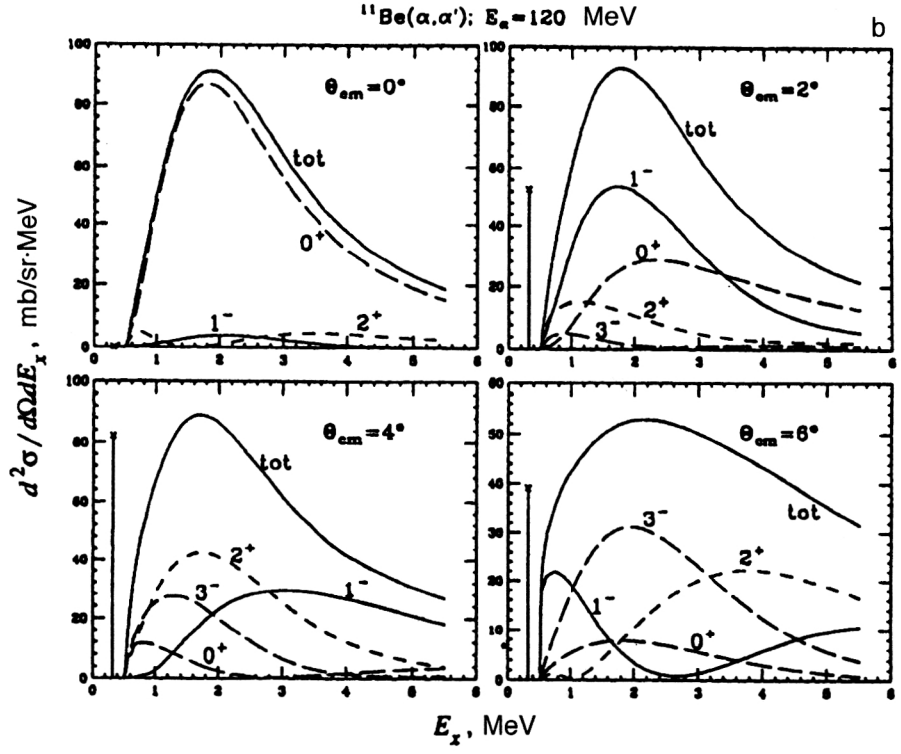


FIG. 14b. (*Continued.*)

experimental errors. In addition, the problem of separating the contributions of processes with excitation of target-nucleus states from the elastic scattering cross sections does not arise in such experiments.

The experimental data have been analyzed using the macroscopic and microscopic optical models and the eikonal and Glauber approximations. The use of the standard optical model with potentials of Woods–Saxon form has shown that it is not possible to obtain a reasonable description of the experimental cross sections using the values of the potential parameters taken from the systematics for stable adjacent nuclei.

The use of microscopic approaches—the optical model with microscopic potentials and the Glauber theory—requires the construction of the matter density distributions in the nucleus using nuclear-structure models. It is reasonable to use a model in which the neutron and proton densities for the target and projectile nuclei are calculated within a single scheme. At the present time such a scheme has been realized using the density-functional method of the theory of finite Fermi systems.

On the whole, the microscopic approaches lead to a reasonable description of the experimental data on the elastic and quasielastic scattering of light exotic nuclei, but in some cases there are serious discrepancies between theory and experiment (for example, for $^{11}$Li+$^{12}$C at $E/A=60$ MeV/nucleon; $^{8}$B+$^{12}$C at $E/A=40$ MeV/nucleon; $^{12}$Be and $^{14}$Be+$^{12}$C at $E/A=56$ MeV/nucleon). The various microscopic models give equally good descriptions of experiment, and differences from the cross sections predicted by theory are observed either at angles where the experimental errors are large, or at scattering angles which are presently inaccessible to measurement. Nevertheless, for most models it is preferable to describe the experimental data using information about the considerable extent of the neutron density tail in $^{8}$He and $^{11}$Li and the proton density tail in $^{7}$Be and $^{8}$B, which confirms the hypothesis of a neutron halo in $^{8}$He and $^{11}$Li and a sizable proton skin in $^{7}$Be and $^{8}$B. However, at present the quality of the experimental data and the level of development of the theoretical models do not allow information about the structure of the neutron (proton) halo and details of the proton and neutron distributions in nuclei to be extracted from analysis of the quasielastic and elastic scattering of light exotic nuclei.

Therefore, the following areas are especialy important in the study of the quasielastic scattering of light exotic nuclei. In experiment: (1) extension of the angular range in measuring the angular distributions; (2) separation of the contribution of inelastic scattering processes from the elastic scattering cross sections; (3) experimental study of the contribution of the soft excitation mode to the scattering cross section; (4) measurement of the angular distributions of the elastic scattering of isobars on the same target nucleus with $N\neq Z$ in order to analyze the isospin dependence of the optical potential and the role of differences in the neutron and proton distributions in the projectile; (5) simultaneous measurement of the angular distributions and the total reaction cross sections at the same energy; (6) study of, in addition to scattering, charge-exchange processes and processes involving nucleon transfer, the cross sections for which can be sensitive to the matter distribution in exotic nuclei. In theory: (1) construction of the polarization potential at the microscopic level; (2) microscopic parameter-free calculation of the absorption potential; (3) analysis of the approximations of the Glauber theory, particularly at low energies ($E/A<30$ MeV/nucleon); (4) theoretical description of the

soft excitation mode and its contribution to the scattering cross section; (5) use of the density-matrix technique to develop a theoretical formalism for describing inelastic and charge-exchange processes, and also reactions involving nucleon transfer; (6) understanding of the relative role played by one-particle and cluster degrees of freedom in forming the properties of light exotic nuclei.

In conclusion, the authors thank S. A. Goncharov, S. N. Ershov, A. A. Ogloblin, Yu. É. Penionzhkevich, and N. K. Skobelev for useful, fruitful discussions about the problems discussed in this study.

One of the authors (S.F.) is grateful to D. Zawischa for interesting and important discussions. His work was partially supported by the Deutsche Forschungsgemeinschaft (DFG).

[1] I. Tanihata, in *Treatise on Heavy-Ion Science*, Vol. 8, edited by D. A. Bromley (Plenum, New York, 1989), p. 443.
[2] C. Detraz and D. J. Vietra, Ann. Rev. Nucl. Part. Sci. **39**, 407 (1989).
[3] E. Roeckl, Rep. Prog. Phys. **55**, 1661 (1992).
[4] C. A. Bertulani, L. F. Canto, and M. S. Hussein, Phys. Rep. **226**, 281 (1993).
[5] T. Minamisono, T. Ohtsubo, I. Minami *et al.*, Phys. Rev. Lett. **69**, 2058 (1992).
[6] G. R. Satchler, K. W. McVoy, and M. S. Hussein, Nucl. Phys. A **522**, 621 (1991).
[7] K. Riisager, Rev. Mod. Phys. **66**, 1105 (1994).
[8] I. Tanihata, J. Phys. G **22**, 157 (1996).
[9] M. Lewitowicz, C. Borcea, F. Carstoiu *et al.*, Nucl. Phys. A **562**, 301 (1993).
[10] J. J. Kolata, M. Zahar, R. Smith *et al.*, Phys. Rev. Lett. **69**, 2631 (1992).
[11] M. Zahar, M. Belbot, J. J. Kolata *et al.*, Phys. Rev. C **49**, 1540 (1994).
[12] I. Pecina, R. Anne, D. Bazin *et al.*, Phys. Rev. C **52**, 191 (1995).
[13] C. B. Moon *et al.*, Phys. Lett. B **297**, 39 (1992).
[14] A. A. Korsheninnikov *et al.*, Phys. Lett. B **316**, 38 (1993).
[15] A. A. Korsheninnikov, E. Yu. Nikolskii, T. Kobayashi *et al.*, Phys. Rev. C **53**, R537 (1996).
[16] S. Neumaier *et al.*, in *Proc. of the Intern. Conf. on Exotic Nuclei and Atom Masses*, Arles, France, June, 1995, *Abstracts of Contr. Papers*, p. B6.
[17] S. Neumaier, G. D. Alkhazov, M. N. Antonenko *et al.*, Preprint GSI-94-43 (1994).
[18] M. D. Cortina-Gil, P. Roussel-Chomaz, L. Alamanos *et al.*, Preprint GANIL P95-16 (1995).
[19] G. R. Satchler, *Direct Nuclear Reactions* (Oxford University Press, Oxford, 1983).
[20] S. A. Fayans, O. M. Knyazkov, I. N. Kuchtina *et al.*, Phys. Lett. B **357**, 509 (1995).
[21] R. J. Glauber, *Lectures in Theoretical Physics*, Vol. 1 (Interscience, New York, 1959), p. 315.
[22] A. V. Smirnov, S. V. Tolokonnikov, and S. A. Fayans, Yad. Fiz. **48**, 1661 (1988) [Sov. J. Nucl. Phys. **48**, 995 (1988)].
[23] H. Feshbach, Ann. Phys. (N.Y.) **5**, 357 (1958).
[24] H. Feshbach, Ann. Phys. (N.Y.) **19**, 287 (1962).
[25] O. M. Knyaz'kov, Fiz. Élem. Chastits At. Yadra **17**, 318 (1986) [Sov. J. Part. Nucl. **17**, 137 (1986)].
[26] Dao Tien Khoa and O. M. Knyaz'kov, Fiz. Élem. Chastits At. Yadra **21**, 1456 (1990) [Sov. J. Part. Nucl. **21**, 623 (1990)].
[27] A. K. Chaudhuri, D. N. Basu, and B. Sinha, Nucl. Phys. A **439**, 415 (1985).
[28] X. Campi and A. Bouyssy, Phys. Lett. B **73**, 263 (1978).
[29] B. Z. Georgiev and R. S. Mackintosh, Nucl. Phys. A **307**, 377 (1978).
[30] O. M. Knyaz'kov and A. A. Nekrasov, Yad. Fiz. **38**, 36 (1983) [Sov. J. Nucl. Phys. **38**, 20 (1983)].
[31] O. M. Knyaz'kov, Izv. Akad. Nauk SSSR, Ser. Fiz. **49**, 928 (1985) [Bull. Acad. Sci. USSR, Phys. Ser.].
[32] E. Fretwurst, G. Lindström, K. F. Reden *et al.*, Nucl. Phys. A **468**, 247 (1987).
[33] O. M. Knyaz'kov and I. N. Kukhtina, Yad. Fiz. **45**, 1604 (1987) [Sov. J. Nucl. Phys. **45**, 995 (1987)].
[34] Dao Tien Khoa, O. M. Knyaz'kov, I. N. Kukhtina, and G. A. Feofilov, Yad. Fiz. **50**, 80 (1989) [Sov. J. Nucl. Phys. **50**, 50 (1989)].
[35] Dao Tien Khoa and O. M. Knyaz'kov, Yad. Fiz. **47**, 1246 (1988) [Sov. J. Nucl. Phys. **47**, 793 (1988)].
[36] Dao Tien Khoa and O. M. Knyaz'kov, Z. Phys. A **328**, 67 (1987).
[37] Dao Tien Khoa, Nucl. Phys. A **484**, 376 (1988).
[38] H. G. Bohlen, E. Stilliaris, B. Gebauer *et al.*, Preprint HMI 1992/P2-Boh 3, Berlin (1992).
[39] A. S. Demyanova, H. G. Bohlen, B. Gebauer *et al.*, Nucl. Phys. A **553**, 727 (1993).
[40] A. M. Lane, Nucl. Phys. **35**, 676 (1962).
[41] S. D. Schery, in *The (p,n) Reaction and the Nucleon–Nucleon Force*, edited by C. D. Goodman *et al.* (Plenum, New York, 1980), p. 409.
[42] O. M. Knyaz'kov, Izv. Akad. Nauk SSSR, Ser. Fiz. **50**, 2007 (1986) [Bull. Acad. Sci. USSR, Phys. Ser.].
[43] O. M. Knyaz'kov and A. A. Kolozhvari, Izv. Akad. Nauk SSSR, Ser. Fiz. **57**, 48 (1993) [Bull. Acad. Sci. USSR, Phys. Ser.].
[44] O. M. Knyaz'kov, A. A. Kolozhvari, I. N. Kukhtina, and S. A. Fayans, Yad. Fiz. **59**, 466 (1996) [Phys. At. Nucl. **59**, 439 (1996)].
[45] S. A. Goncharov, O. M. Knyaz'kov, and A. A. Kolozhvari, Yad. Fiz. **59**, 666 (1996) [Sov. J. Nucl. Phys. **59**, 634 (1996)].
[46] S. Shimoura, in *Proc. of the Intern. Conf. on Exotic Nuclei and Atom Masses*, Arles, France, June, 1995, *Abstracts of Contr. Papers*, p. B5.
[47] G. Bertsch, J. Borysowicz, H. McManus *et al.*, Nucl. Phys. A **284**, 399 (1977).
[48] F. Petrovich, H. McManus, V. A. Madsen *et al.*, Phys. Rev. Lett. **22**, 895 (1969).
[49] G. R. Satchler and W. G. Love, Phys. Rep. **55**, 183 (1979).
[50] A. M. Kobos, B. A. Brown, P. E. Hodgson *et al.*, Nucl. Phys. A **384**, 65 (1982).
[51] A. M. Kobos, B. A. Brown, R. Lindsay *et al.*, Nucl. Phys. A **425**, 205 (1984).
[52] J.-P. Jeukenne, A. Lejeune, and C. Mahaux, Phys. Rev. C **16**, 80 (1977).
[53] Dao Tien Khoa, G. R. Satchler, and W. von Oertzen, Phys. Lett. B **358**, 14 (1995).
[54] S. N. Ershov, F. A. Gareev, and H. Lenske, Preprint E4-95-408, JINR, Dubna (1995).
[55] J. S. Al-Khalili and J. A. Tostevin, Phys. Rev. C **49**, 386 (1994).
[56] Dao Tien Khoa, G. R. Satchler, and W. von Oertzen, Phys. Rev. C **51**, 2069 (1995).
[57] M. S. Hussein and G. R. Satchler, Nucl. Phys. A **567**, 165 (1994).
[58] S. A. Goncharov and A. A. Ogloblin, Yad. Fiz. **56**, No. 3, 40 (1993) [Phys. At. Nucl. **56**, 309 (1993)].
[59] A. G. Sitenko, Ukr. Fiz. Zh. **4**, 152 (1957) [in Russian].
[60] I. Tanihata, H. Hamagaki, O. Hashimoto *et al.*, Phys. Rev. Lett. **55**, 2676 (1985).
[61] B. Blank *et al.*, Z. Phys. A **343**, 375 (1992).
[62] F. A. Gareev, S. N. Ershov, G. S. Kazacha *et al.*, Report E4-92-458, JINR, Dubna (1992) [in Russian].
[63] L. J. Thompson *et al.*, Phys. Rev. C **47**, 1364 (1993).
[64] J. S. Al-Khalili *et al.*, Nucl. Phys. A **581**, 331 (1995).
[65] F. A. Gareev, S. N. Ershov, G. S. Kazacha *et al.*, Yad. Fiz. **58**, 620 (1995) [Phys. At. Nucl. **58**, 564 (1995)].
[66] S. A. Fayans, Phys. Lett. B **267**, 443 (1991).
[67] M. V. Zhukov, B. V. Danilin, D. V. Fedorov *et al.*, Phys. Rep. **231**, 151 (1993).
[68] D. Baye, P. Descouvemont, and N. K. Timofeyuk, Nucl. Phys. A **577**, 624 (1994).
[69] A. Csótó, Phys. Lett. B **315**, 24 (1993).
[70] K. Varga and Y. Suzuki, Phys. Rev. C **52**, 2885 (1995).
[71] P. Hohenberg and W. Kohn, Phys. Rev. B **136**, 864 (1964).
[72] W. Kohn and L. Sham, Phys. Rev. A **140**, 1133 (1965).
[73] S. A. Fayans and V. A. Khodel', Pis'ma Zh. Éksp. Teor. Fiz. **17**, 633 (1973) [JETP Lett. **17**, 444 (1973)].
[74] É. E. Sapershteĭn, S. A. Fayans, and V. A. Khodel', Fiz. Élem. Chastits At. Yadra **9**, 221 (1978) [Sov. J. Part. Nucl. **9**, 91 (1978)]; S. A. Fayans, E. E. Saperstein, and V. A. Khodel, Nucl. Phys. A **317**, 424 (1979); V. A. Khodel and E. E. Saperstein, Nucl. Phys. A **348**, 261 (1980).
[75] V. A. Khodel and E. E. Saperstein, Phys. Rep. **92**, 185 (1982).
[76] D. Vautherin, D. M. Brink *et al.*, Phys. Rev. C **5**, 626 (1972).
[77] S. A. Fayans, S. V. Tolokonnikov, E. L. Trykov, and D. Zawischa, Phys. Lett. B **338**, 1 (1994).
[78] I. Tanihata, T. Kobayashi, O. Yamakawa *et al.*, Phys. Lett. B **206**, 592 (1988).
[79] I. Tanihata, T. Kobayashi, T. Suzuki *et al.*, Phys. Lett. B **287**, 307 (1992).

[80]G. F. Bertsch, B. A. Brown, and H. Sagawa, Phys. Rev. C **39**, 1154 (1989).
[81]H. de Vries, C. W. de Jager, and C. de Vries, At. Data Nucl. Data Tables **36**, 495 (1987).
[82]H. G. Bohlen *et al.*, Z. Phys. A **322**, 241 (1993).
[83]P. M. Endt and C. van der Leun, Nucl. Phys. A **310**, 1 (1978).
[84]F. Ajzenberg-Selove, Nucl. Phys. A **506**, 1 (1990).
[85]J. Raynal, in *Proc. of the Workshop on Applied Nuclear Theory and Nuclear Model Calculations for Nuclear Technology*, Trieste, Italy, 1988, edited by M. K. Mehto and J. J. Schmidt (World Scientific, Singapore, 1988), p. 506.
[86]F. Carstoiu and M. Lassaut, Nucl. Phys. A **597**, 269 (1996).
[87]M. C. Mermaz, Phys. Rev. C **47**, 2213 (1993).
[88]R. Da Silveira, S. Klarsfeld, A. Boukour, and Ch. Leclercq-Willain, Phys. Rev. C **48**, 468 (1993).
[89]K. Yabana *et al.*, Nucl. Phys. A **539**, 295 (1992).
[90]J. S. Al-Khalili *et al.*, Nucl. Phys. A **581**, 316 (1995).
[91]C. A. Bertulani and H. Sagawa, Nucl. Phys. A **588**, 667 (1995).
[92]G. R. Satchler and M. S. Hussein, Phys. Rev. C **49**, 3350 (1994).
[93]E. Stiliaris *et al.*, Phys. Lett. B **223**, 291 (1989).
[94]R. Da Silveira, S. Klarsfeld, A. Boukour, and Ch. Leclercq-Willain, Phys. Rev. C **51**, 1572 (1995).
[95]C. B. Moon, M. Fujimaki, S. Hirenzaki *et al.*, Preprint RIKEN-AF-NP-126, RIKEN, Japan (1992).
[96]S. Hirenzaki *et al.*, Nucl. Phys. A **552**, 57 (1993).
[97]M. Kohno, Phys. Rev. C **48**, 1322 (1993).
[98]P. Roussel-Chomaz, N. Alamanos, and P. Delbourgo-Salvador, Preprint GANIL P95-09 (1995).
[99]Y. Suzuki, K. Yabana, and Y. Ogawa, Phys. Rev. C **47**, 1317 (1993).
[100]A. K. Chaudhuri, Phys. Rev. C **49**, 1603 (1994).
[101]R. L. Varner, W. J. Thompson, T. L. McAbee *et al.*, Phys. Rep. **201**, 57 (1991).
[102]F. Brieva and J. R. Rook, Nucl. Phys. A **291**, 299 (1977).
[103]N. Yamaguchi, S. Nagata, and T. Matsuda, Prog. Theor. Phys. **70**, 459 (1983).
[104]S. A. Goncharov and A. A. Korsheninnikov, Preprint RIKEN-AF-NP-163, RIKEN, Japan (1993).
[105]S. A. Goncharov and A. A. Korsheninnikov, Yad. Fiz. **58**, 1393 (1995) [Phys. At. Nucl. **58**, 1311 (1995)].
[106]M. V. Zhukov, A. A. Korsheninnikov, and M. S. Smedberg, Phys. Rev. C **50**, R1 (1994).
[107]W. D. Myers, Nucl. Phys. A **204**, 465 (1973).
[108]W. D. Myers and K.-H. Schmidt, Nucl. Phys. A **410**, 61 (1983).
[109]J. H. Sorensen and A. Winther, Nucl. Phys. A **550**, 329 (1992).
[110]L. V. Chulkov, C. A. Bertulani, and A. A. Korsheninnikov, Nucl. Phys. A **587**, 291 (1995).
[111]I. Tanihata, Nucl. Phys. A **478**, 795c (1988).
[112]M. C. Mermaz, Phys. Rev. C **50**, 2620 (1994).
[113]T. Yamagata, K. Yuasa *et al.*, Phys. Rev. C **39**, 873 (1989).
[114]S. A. Fayans, A. P. Platonov, G. Graw, and D. Hofer, Nucl. Phys. A **577**, 557 (1994).
[115]A. C. C. Villari *et al.*, Phys. Lett. B **268**, 345 (1991).
[116]R. E. Warner *et al.*, Phys. Rev. C **52**, R1166 (1995).
[117]M. E. Brandan and G. R. Satchler, Nucl. Phys. A **487**, 477 (1988).
[118]S. Kox, A. Gamp *et al.*, Phys. Lett. B **159**, 15 (1985).
[119]O. M. Knyaz'kov, I. N. Kukhtina, and S. A. Fayans, in *Abstracts of Reports Presented at the Intern. Conf. on Nuclear Spectroscopy and Nuclear Structure* [in Russian] (Nauka, Moscow, 1996), p. 101.
[120]I. N. Efimov, Yad. Fiz. **12**, 1080 (1970) [Sov. J. Nucl. Phys. **12**, 589 (1971)]; Commun. Nucl. Part. Phys. **19**, 271 (1990).
[121]A. B. Migdal, Yad. Fiz. **16**, 427 (1972) [Sov. J. Nucl. Phys. **16**, 238 (1973)].
[122]H. Sagawa, in *Proc. of the Intern. Symp. on Structure and Reactions of Unstable Nuclei*, Niigata, 1991, edited by K. Ikeda and Y. Suzuki (World Scientific, Singapore, 1992), p. 149.
[123]S. A. Fayans, S. N. Ershov, and E. F. Svinareva, Phys. Lett. B **292**, 239 (1992).
[124]Nguyen Van Giai, Phys. Lett. B **105**, 11 (1981).
[125]S. A. Fayans, V. V. Palichik, and N. I. Pyatov, Z. Phys. A **308**, 145 (1982).
[126]N. K. Timofeyuk, D. Baye, and P. Descouvemont, Nucl. Phys. A **551**, 1 (1993).
[127]B. V. Danilin, I. J. Thompson, M. V. Zhukov *et al.*, Phys. Lett. B **333**, 299 (1994).
[128]H. Sagawa, N. Van Giai, N. Takigawa *et al.*, Z. Phys. A **351**, 385 (1995).
[129]J. R. Comfort and B. C. Karp, Phys. Rev. C **21**, 2162 (1980).
[130]W. G. Love, in *The (p,n) Reaction and the Nucleon–Nucleon Force*, edited by C. D. Goodman, S. M. Austin, S. D. Bloom *et al.* (Plenum, New York, 1979), p. 23.
[131]W. G. Love and M. A. Franey, Phys. Rev. C **24**, 1073 (1981); **31**, 488 (1985).
[132]E. Fabrici *et al.*, Phys. Rev. C **21**, 844 (1980).
[133]S. M. Smith *et al.*, Nucl. Phys. A **207**, 273 (1973).
[134]C. A. Bertulani and H. Sagawa, Phys. Lett. B **300**, 205 (1993).

Translated by Patricia A. Millard